sustainability

MDPI

Article

Geospatial Analysis for Relative Seismic Activity Assessment: A Case Study of Fatima Suture Zone in Western Saudi Arabia

Bashar Bashir * and Abdullah Alsalman

Department of Civil Engineering, College of Engineering, King Saud University, P.O. Box 800, Riyadh 11421, Saudi Arabia
* Correspondence: bbashir@ksu.edu.sa

Abstract: In this paper, we state the usefulness of geomorphic analysis, typically applied to highly deformed landforms, to investigate the tectonic geomorphology of an intercontinental structure: the Fatima suture zone. The Fatima suture zone (FSZ) landscape is a tectonically distinct deformation zone along the eastern coast of the Red Sea in western Saudi Arabia providing a complex zone in terms of geology, tectonics, and geomorphology. This zone presents many deformations and fault reactivations that were produced from the effect of horizontal, vertical, and thrust motions as well as deposition and erosion processes. Through several morphometric analyses, remotely sensed data, and geospatial techniques, we recognized the detailed geomorphic surface features of the Fatima suture zone region. Morphometric indices applied in this paper include the stream length gradient index (*SL*), basin asymmetry factor index (*Af*), hypsometric integral index (*Hi*), valley floor width to valley floor height ratio index (*Vf*), basin shape index (*Bs*), and mountain front sinuosity index (*Smf*). Every single morphometric index provides three different relative tectonic classes based on the assigned value ranges. The overall results obtained from the analysis were averaged and presented as an indicator index namely the relative seismic activity (RSA) index, which was classified into four distinct classes from relatively very high to low seismic activity: class 1 is very high seismic activity (CA $\leq$ 1.5); class 2 is high seismic activity (1.5 < CA $\leq$ 2); class 3 is moderate seismic activity (2 < CA $\leq$ 2.5); and class 4 is low seismic activity (CA > 2.5). Additionally, a combination of the two indices (*Smf* and *Vf*) was presented as a quantitative model of the relative seismic activity of the examined mountain fronts. The results of the RSA index provided signatures of all four classes of the study region. Two-thirds of the total area of the study region were recorded as high to very high classes in terms of seismic activity. The paper finally concludes that this integration method allows assessment and evaluation of the highly deformed landscapes related to active tectonism. Despite the impact of the Fatima suture zone providing low to medium activities in some parts, it has a signature control on the recent landscape evolution.

Keywords: geomorphic indices; active tectonics; geospatial analysis; Fatima suture zone; Saudi Arabia

Citation: Bashir, B.; Alsalman, A. Geospatial Analysis for Relative Seismic Activity Assessment: A Case Study of Fatima Suture Zone in Western Saudi Arabia. *Sustainability* **2023**, *15*, 11130. https://doi.org/10.3390/su151411130

Academic Editors: Büyüksaraç Aydın and Işık Ercan

Received: 5 June 2023
Revised: 5 July 2023
Accepted: 12 July 2023
Published: 18 July 2023

1. Introduction

Tectonic geomorphology presents one of the most expanding disciplines integrating tectonics and geomorphology. As the geological branch rapidly develops, it is likely that more attention will be given to quantifying the rates, timing, and magnitude of different landscape evolutions [1]. It is also suggested to incorporate the study of geochronology, geophysics, geodesy, paleoclimatology, remote sensing, and archology, among others [2–5]. This geological trend is very significant because the quantifying results of regional research on neo-tectonism are important for precisely evaluating land use development and natural hazards management of heavily populated regions [2,6]. In mountain regions, recent tectonic activity can be expressed as a major reason for the reshaping of the different landforms of Earth's surface as the product of the interaction between erosional and tectonic actions [2,7,8]. The study of drainage system behaviors in active regions proves that it is

able to understand tectonic evolution and present tectonic signatures [3]. They can be recognized from river slope, river incision rate, basin geometry, and river path deflection [9–11]. The morphometric indices identify morphometric surfaces that present evidence of recent tectonic activity of different landforms [11–13]. The Tertiary rift of the Red Sea is situated between the African and Arabian Shields (Figure 1a). Morphometric analysis has broadly been successfully used in several different tectonically active regions. Globally, many studies applied this analysis including Central USA [14], northern Mississippi (USA) [15], California (USA) [16], southern Italy [17], southern Spain [9], Germany [18], eastern Turkey [19,20], and central Greece [21]. On the other hand, this effective analysis was successfully applied locally, including in the eastern desert of Egypt [22], southeastern Iran [23], southwestern Iran [24], the Gulf of Suez [25], the Sinai Peninsula [26], eastern Jordan [27], and central Arabia [28]. The tectonic story of the Arabian Shield was initiated by the spreading of the Red Sea producing different types of arcs during the rifting processes of Rodinia [29]. Recent active tectonism associated with surface uplift is recognized along the eastern border of the Red Sea basin in western Saudi Arabia via faulted blocks, deeply incised streams, and quaternary deposits along the Red Sea margin zone [30–32]. The seismic record of the Red Sea provides all earthquake magnitudes ($M \geq 2{:}7$) from 1964 to the present day including earthquakes not presented by *ISC* (http://www.isc.ac.uk (accessed on 26 March 2023) [33–35]. The Fatima suture zone provides a natural laboratory for investigating continental-scale thrusting systems (Figure 1b). Studying active tectonics along those regions with high relative tectonic signals during the Holocene and late Pliocene is extremely important and significant to evaluate recent tectonic activity and regional seismic hazard possibilities [12,36,37]. Investigating regional areas to calculate active tectonic rates or even applying quantitative methods to obtain those rates is very critical, and such investigations are always in need of modern data and methods [9,15,19].

The general approach of this work is to focus on the geomorphic signatures of the active tectonic intercontinental suture zone in Jeddah terrane at the western Arabian Shield. Thus, standard morphometric indices that are known to be very effective in tectonic geomorphology studies [6,23,38–40] including the stream length gradient index (*SL*), basin asymmetry factor index (*Af*), hypsometric integral index (*Hi*), valley floor width to valley floor height ratio index (*Vf*), basin shape index (*Bs*), and mountain front sinuosity index (*Smf*) were applied and calculated. The main purpose of this work is to preciously apply and calculate several morphometric indices of relative tectonism and topographic signatures to provide an average single index reference that aids in mapping and categorizing the different relative tectonic scales of the Fatima suture zone (FSZ). Based on the combined analysis of the valley floor width to valley height (*Vf*) and mountain front sinuosity (*Smf*) indices, this paper also aims to present a classification of relative tectonic scales for each structural segment and the seismic potential of the entire Fatima suture zone for the regional seismic hazards. Under this framework process, the paper additionally aims to prove the validity of the morphometric analysis, typically used in active regions to evaluate the tectonic signature and development of landscapes.

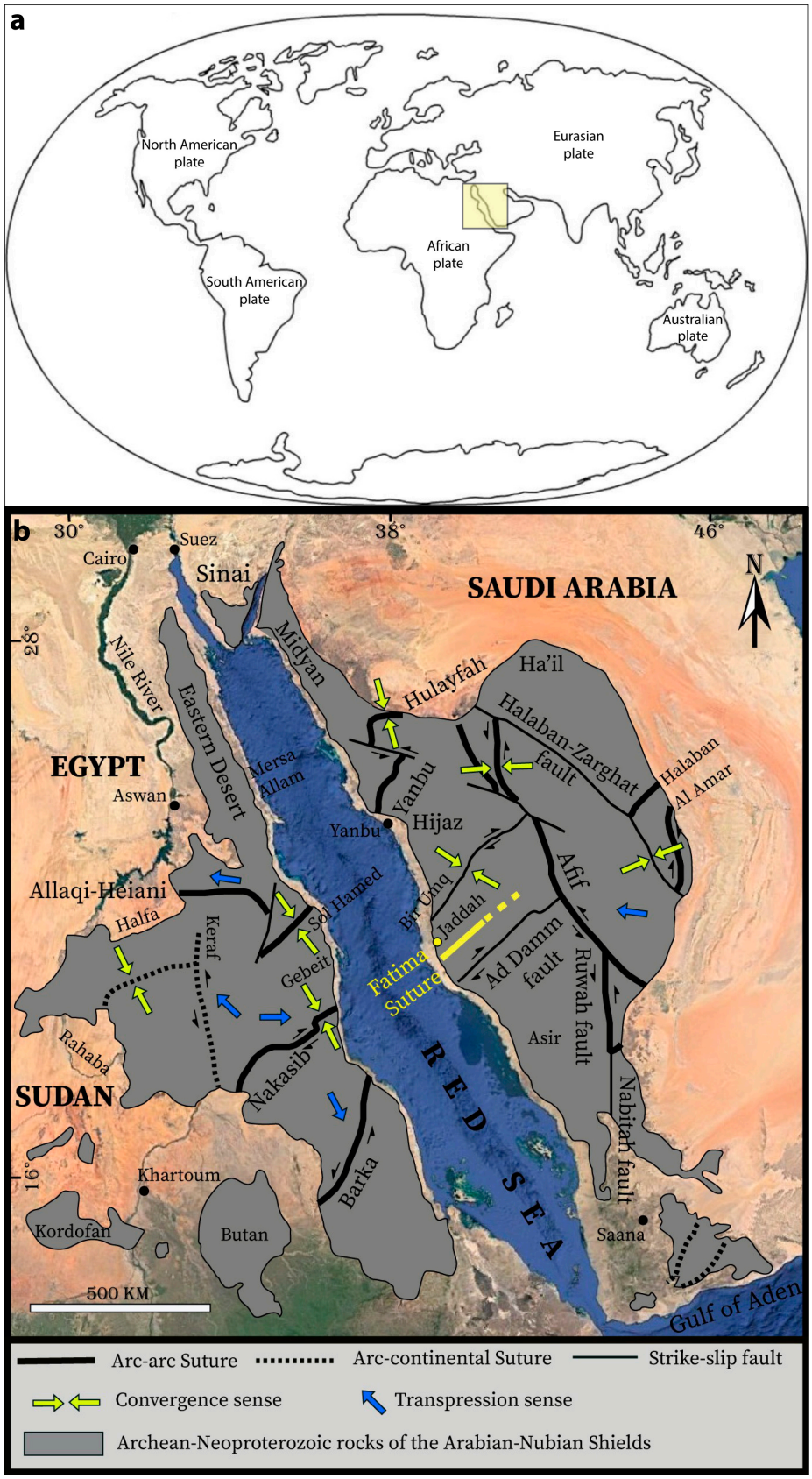

Figure 1. (**a**) A simplified plate tectonic map showing the location of the Arabian–Nubian Shield. (**b**) Simplified tectonic setting map of the Arabian–Nubian Shield illustrating faults and sutures of the different tectonic terrenes.

2. Regional Geological and Structural Setting

The Fatima suture zone (FSZ) has been deformed from highly thrusted mafic, ultramafic, and volcanic-sedimentary rocks. It is a very complex region in terms of geology, tectonics, and geomorphology (Figure 1b). It is located between the Ad Damm fault zone and bi'r Umq suture zone (Figure 1) in a border deformation zone along the eastern coast of the Red Sea basin. The study region is ~17.192 km^2 within the zone of Jeddah terrane [41,42]. A complete sequence of the ophiolite has been mapped in the FSZ presenting a northeast–southwest trend in the western zone of the Arabian Shield [42]. The geological investigation in the FSZ indicates that the described ophiolitic section is metamorphosed to amphibolite and green-schist facies and is intruded by later felsic and mafic intrusions [41]. The oldest unit that has been observed in the FSZ belongs to the Precambrian period and is located at the southeastern corner of the FSZ region. It is described as the Wadi Lithis series, which is composed of a metamorphic complex of meta-diorite, meta-gabbro, and amphibolite. Unconformable, the Precambrian amphibolite schist layers overlie the Wadi Litho series. They include some beds of marble, sericite schist, and quartzite [41]. The sericite and chlorite schist is derived mostly from sediments and has been recorded in the eastern part of the study region covering a very narrow elongated zone. This unit belongs to the Precambrian age as well. It is described as quarzitic stretched conglomerate, minor arkosite, graphitic schist, and marble [43]. The Precambrian andesite, diabase, slate, greenstone conglomerate is intercalated with andesite porphyry and mostly presents sharp contact with the southern part of the Mecca batholith. It is also observed north of the FSZ structure [43]. Unconformable, the diorite and granodiorite unit was mainly observed in the southern part of the FSZ and is composed of gneissic, some sheared and altered quartz diorite, and adamellite. It is often contaminated with migmatitic xenolithic metamorphic rocks [43,44]. The Mecca batholith at both exposures of the Fatima suture covers granite, granite gneiss, granodiorite, gabbro, tonalite, and diorite, locally mylonitized and foliated in the areas exposed near the Fatima shear zone [41]. Authors in Ref. [45] described the tonalite as having a well-foliated gneissic texture with well-segregated layers of felsic and mafic minerals [41]. Nonconformable, the Halaban andesite unit comes after the granite and granite gneiss unit. Halan andesite is fine-grained andesite and felsite, subordinate dacite, trachyte, and rhyolite breccia and agglomerate in extrusive phase [43]. Layers of the Fatima Formation were observed and recorded in a post-amalgamation basin [41,43,44]. These layers overlie nonconformably on the volcanic and granitic rocks along the northwestern edges of the FSZ structure [43,46]. The Fatima Formation is composed of arkose, red and purple shale or slate, siltstone, basal conglomerate, sandstone, and thin limestone members containing stromatolitic structures [43]. Red or pink unmetamorphosed alkalic to per-alkalic granite and some grey adamellite were cropped out in the southern part of the study zone [43]. In this suture zone, the Eocene age is represented by the Usfan and Shumaysi Formations. The Usfan Formation is recorded as a very small area in the northeastern corner of the study zone [43]. It is composed mainly of marine and littoral sediments [43]. The Shumaysi Formation overlies conformably on the Usfan Formation. The lithology of the Shumaysi Formation is sandstone, white shale, siltstone, and oolitic hematite [43]. The Pliocene olivine-rich basalt is mapped mainly in the northeastern corner of the study zone. This unit presents lower flow that is in part weathered and dissected; the youngest flows and cinder cones are little altered [41,43]. The quaternary deposits are represented by three types of sediments. Terrace sand and gravel were observed in the northern part of the study zone. The next quaternary deposits are gravel, silt, sand, and clay [43]. They include coastal plain surficial deposits and slightly raised coral reefs. They cover most of the western areas of the study zone [42,43]. The final quaternary deposits are represented by eolian mobile sand covering small elongated areas in the western part of the study zone [43].

Structurally, a complete ophiolitic section has been observed and mapped in the FSZ showing a northeast–southwest direction in the western part of the Arabian Shield [42]. The ophiolitic rocks are deformed by thrust faults and folds and show distinctive styles

and patterns of lineations and foliations [41,42]. Low deformed granitic rocks of the Mecca batholith cover both shoulders of the FSZ structure line, whereas thrust faults having opposite dipping oriented NE control its internal deformations [41]. The intrusion deformation of a pink granitic rock took place along the southeastern shoulder of the FSZ that has been laterally deformed by thrusting between the metagabbro, tonalite, and serpentinite rocks [41,43]. NW- and SE-verging thrust faults in the two edges of the FSZ deformation are joined at its middle part producing a positive flower deformation that presents the uplifting signature of the entire zone [41]. The author in Ref. [47] also recognized the antithetic thrusting and its positive flower structure [41]. Antithetic thrust faults also deform the two margins of the FSZ. The FSZ's main thrusts show steep dips, whereas the nearly vertical intersecting thrust faults give gentle dips [41–43]. Structural analysis that has been applied along the FSZ provides foliation patterns paralleling the thrust traces and records several folds that have different styles and trends [42,45,46]. All details about the lithological and structural framework of the current work are illustrated in Figure 2.

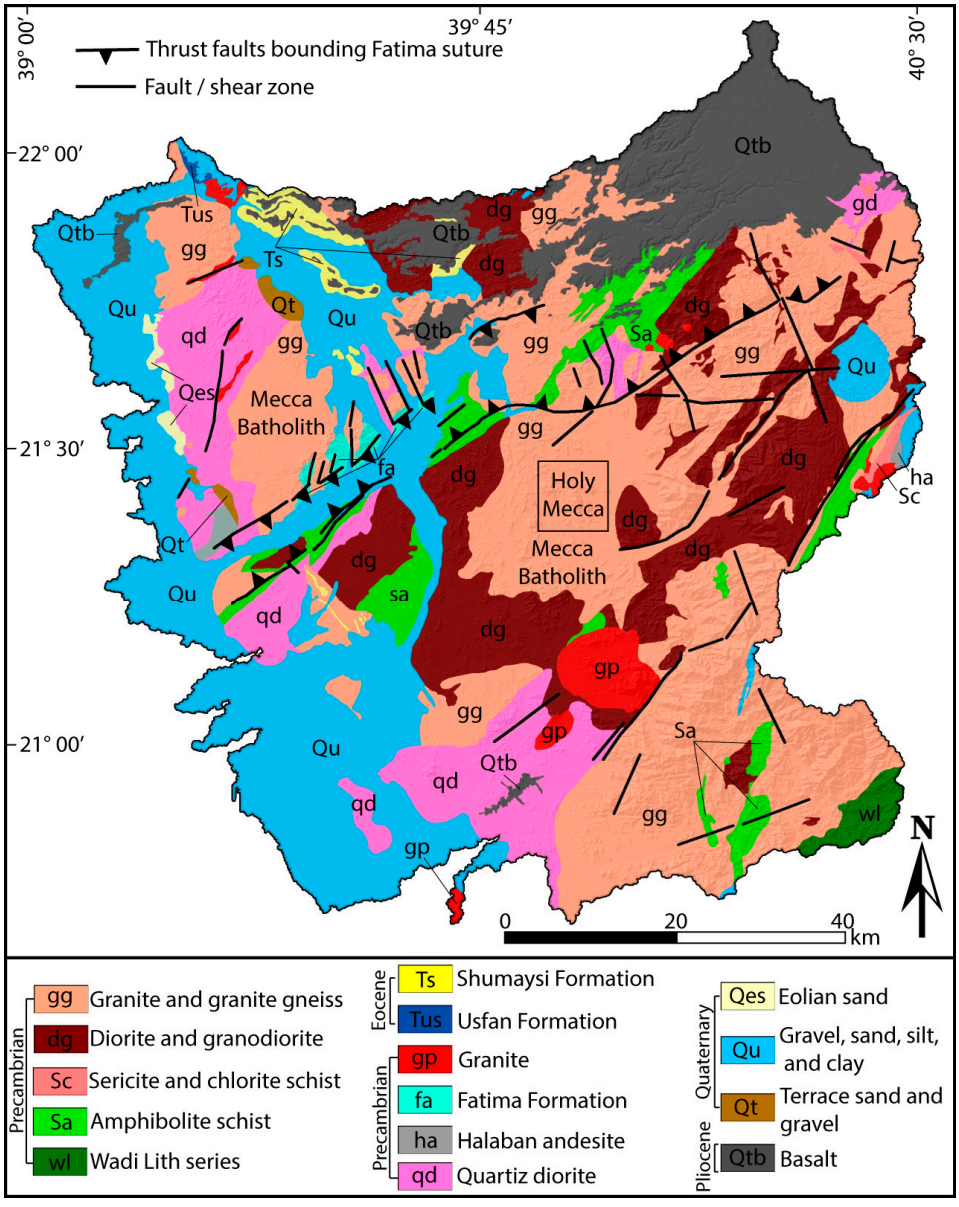

Figure 2. Detailed geological map of the Fatima suture zone and neighboring regions modified after [43].

3. Methodology

In this work, integration between remotely sensed data and geospatial analysis plays the main role in investigating the relative tectonic framework of the FSZ. Applying the different tools in ArcGIS (version 10.4) and QGIS (Version 3.28.5) on a 30 m spatial resolution digital elevation model (DEM) produced from a Shutter Radar Topography Mission (SRTM), morphometric and topographic signatures of the entire FSZ were extracted. Several morphometric indices were examined and calculated over the FSZ within a total region of about 17.192 km^2. The processed hill-shade tool in ArcGIS was run to analyze the valley floor width to valley height and mountain front sinuosity indices. Raster and hydrology analysis options in both ArcGIS and QGIS were used in constructing and classifying the proposed region into numbers of basins that give streams greater than the fourth order by the stream order method of the author in Ref. [48]. The basins, basin sizes, basin delineations, stream orders, and stream drainage systems were extracted and modeled from the possessed digital elevation data through the available algorithms in the software tools used. The basins were ordered from 1 to 41 covering the entire region of the FSZ. The thrusting and accompanying structural elements within the study zone were categorized into 50 segments on the basis of varying trends of the different faults. The investigative morphometric indices are based on lithology type and the quantitative analysis of the drainage systems and mountain front sensuosities [49,50]. These effective indices may provide anomaly values indicating some local changes in the general uplift or subsidence framework [2,9,22]. In the current study, we calculated and analyzed several different morphometric indices in the Fatima suture mountain fronts and neighboring basins. These indices are assigning three relative tectonic classes based on the value ranges of every single morphometric index. Accordingly, the assigned classes are averaged and arbitrarily classified into an index of tectonic activity (ITA) of the entire investigated region. Particularly, Vf and Smf indices are analyzed together to provide an activity calcification of the mountain fronts along the main Fatima suture deformation. Studying the rock strength of deformed regions helps in effectively analyzing most of the morphometric indices [2,3,9,37]. The rock strength of the study region has been inferred and evaluated following field observation and research of authors in similar studies [3,24,39,51]. In this study, several classes or levels of rock resistance were recognized along with the lithology type and field description, starting with very high resistance level (metamorphic complex, marble, quartzite, diorite, and granodiorite); high resistance level (granite, granite gneiss, andesite, and felsite); moderate resistance level (quartz diorite, sandstone, and sandy limestone); and low resistance level (sandstone, conglomerate, shale, marly limestone, and eolian sand).

3.1. Morphometric Indices

3.1.1. Stream-Length Gradient Index (*SL*)

The stream-length gradient index (*SL*) is one of the sensitive tools considered in morphometric analysis [5,19,52]. It is defined as:

$$SL = (\Delta h/\Delta l) \times l$$

where $\Delta h/\Delta l$ describes the local gradient of the stream segment (change in height divided by change in length), and term l represents the length of the segments from the investigated drainage divide to the midpoint of the evaluated river reach [39,52] (Figure 3).

The processing of the *SL* index has been run every 50 m of the length of the rivers and streams. This quantitative index is very indicative for assessing active structure elements, particularly fault segments and their level of activity [9,12,22]. This index depends mainly on the tectonic and lithological controls on river profiles across the fault trace [39]. The SL index values increase as streams and rivers run over resistant rocks and tectonically active areas [12,24] and decrease as rivers flow over less soft rocks and or very low tectonic activity [24].

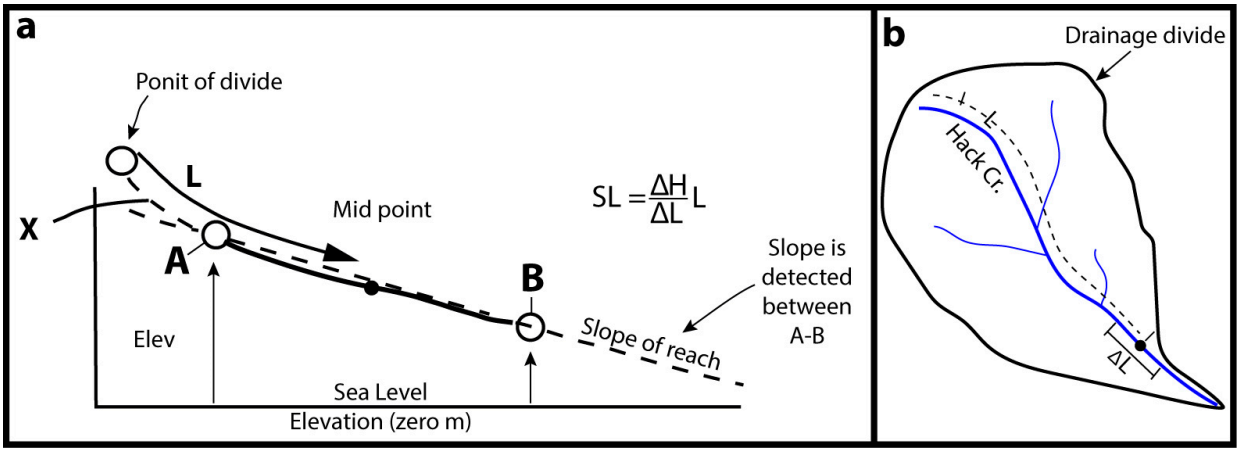

Figure 3. (**a**) Mechanism of the calculation of the SL index and (**b**) Simplified view of the basin modified after that of author in Ref. [52].

3.1.2. Asymmetric Factor (*Af*)

The asymmetrical factor index (*Af*) is a valuable parameter to assess tectonic tilting regarding the scale of an investigated drainage basin [11,12,53]. This index may be calculated over a relatively vast area [53]. The *Af* index is defined as:

$$Af = 100 \times (Ar/At)$$

where *Ar* describes the part facing downstream occupying area to the right of the basin, whereas *At* provides a figure regarding the entire area of the investigated basin (Figure 4). The values of this index are sensitive to variances in tilting perpendicular to the main river direction [9,19]. *Af* values close to 50 provide stable conditions for a basin with no or little tilting, while values below or above 50 could produce, as a result of the tilting level of a basin, tectonic signatures or lithological structures that control erosion processes, as for example rivers going down bedding plains over time [9,19,23]. Regarding this index, structural control of the bedding orientation could play a significant role in basin asymmetry development [2].

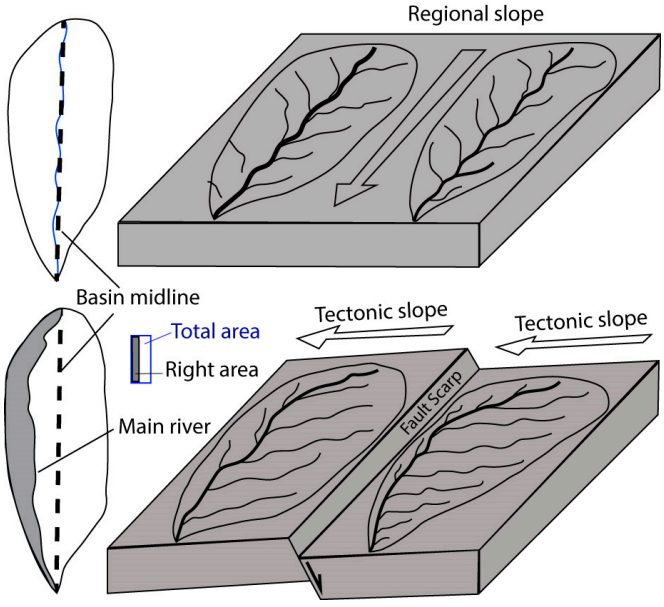

Figure 4. Drainage system response to uplift along a normal fault by moving laterally in a down-tilt direction, modified after authors' work in Ref. [12].

3.1.3. Hypsometric Integral Index (*Hi*)

The hypsometric integral index plays a significant role in tectonic geomorphology studies [1,3]. This integral index is generally extracted for a particular basin and is a parameter that is independent of a given basin total area. It recognizes the distribution of elevation of a given landscape area, particularly a basin [2,48]. The mechanism of this index is run as the zone below the derived hypsometric curve and thus describes the total volume of a given basin that has been assigned for no erosion [9,24] (Figure 5).

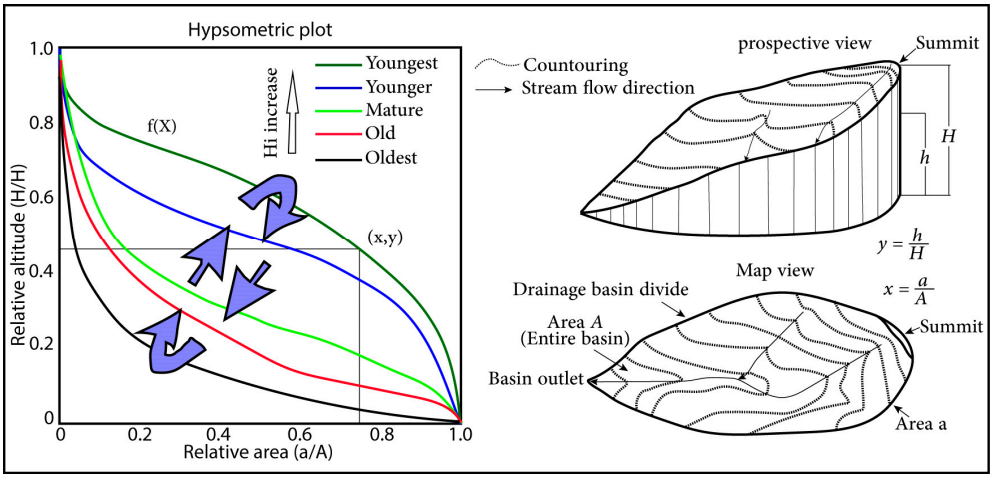

Figure 5. Typical different models of hypsometric curves, after work by author in Ref. [48] and geomorphic process development, after authors' work in Refs. [2,8].

The formula that may be run to define this index [9,12] is:

$$Hi = (\text{Mean elevation} - \text{Min. elevation}/\text{Max. elevation} - \text{Min elevation})$$

The required values for this index are extracted from the SRTM digital elevation model. Significantly, this index works in a similar manner to the SL index in that lithological strength as well as other indices influence the value, and it does not directly indicate tectonic activity signals [9].

3.1.4. Drainage Basin Shape Index (*Bs*)

The shape of the drainage basins may be differentiated between different basins and their activity levels. Accordingly, in active tectonic zones the elongated basins paralleling to the topographic slope of a mountain tend to give signatures about tectonism and are described as relatively younger basins. As tectonic signals cease or revolution continues, the elongated basins convert to circular basins [2,40] (Figure 6).

The horizontal projection of a drainage basin shape may be expressed using the circularity scale; *Bs* [22,54] calculated via the following simple formula:

$$Bs = \text{Bl}/\text{Bw}$$

where Bl measures the length of the drainage basin detected from the basin headwaters to the basin mouth, and Bw describes the basin width at its widest edges. High Bs results indicate basins with elongation shapes reflecting high tectonic activity signals, while low *Bs* results tend to describe basins with more circular shapes and lower tectonic activity levels. Mountain fronts characterized by rapid uplifting generally are recognized by steep and elongated drainage basins, and when tectonism processes slow down, extending basins are produced from the mountain front up [9,54].

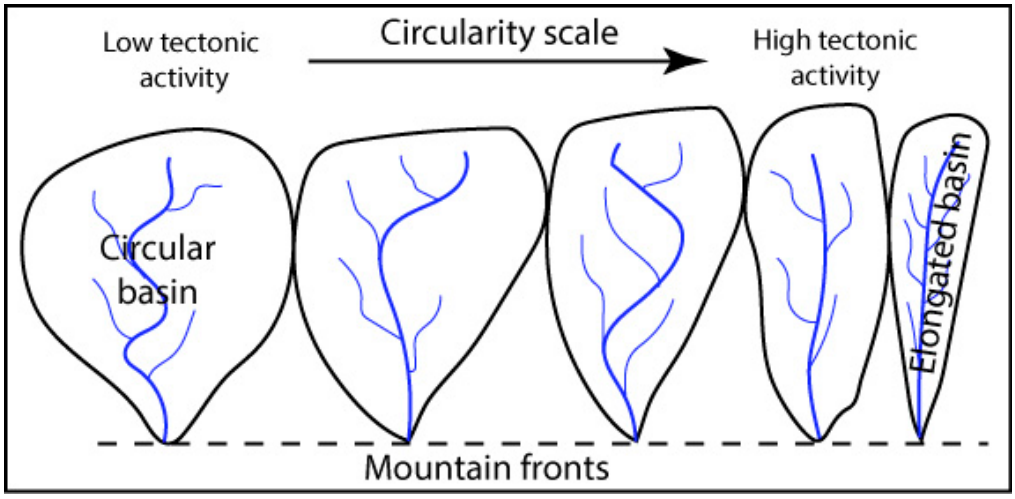

Figure 6. Drainage basin shape scale.

3.1.5. Valley Floor Width-to-Height Index (*Vf*)

The valley floor width-to-height index parameter (*Vf*) is a very significant morphometric indicator that discriminates between the maturity levels of basins [40]. It is recognized as:

$$Vf = 2\text{Vfw}/(\text{Eld} - \text{Esc}) + (\text{Erd} - \text{Esc})$$

where Vfw estimates averaged width of the valley floor; Eld gives values of the elevation of the divide along the left wall of the valley; Erd expresses the right wall averaged elevation; and Esc estimates the elevation of the floor of the valley [3] (Figure 7).

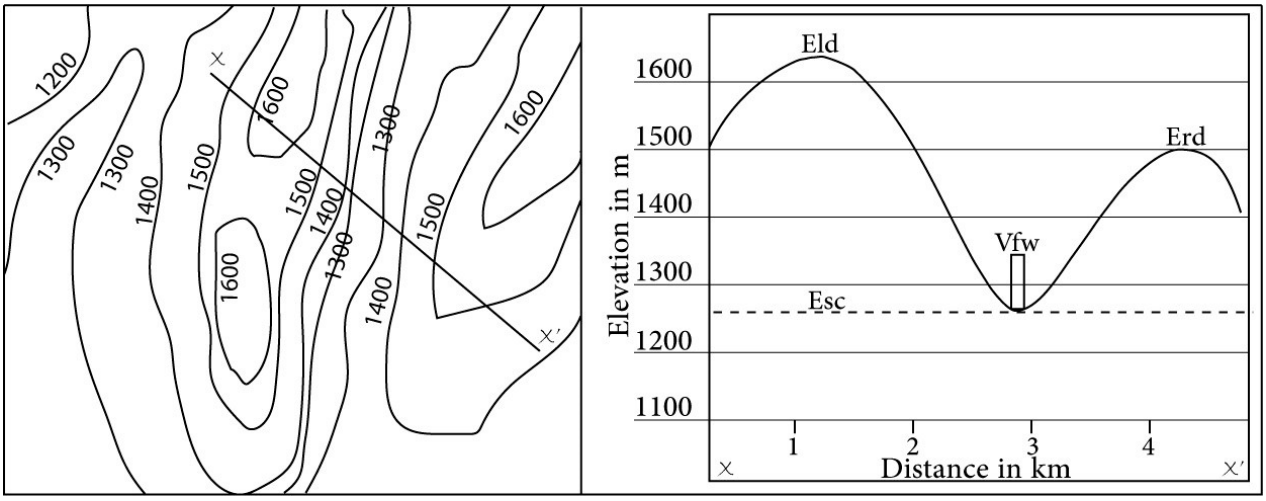

Figure 7. Mechanism of measuring the valley floor width-to-height (*Vf*).

This index mainly records relative uplift and incision rates. It is differentiated between V-shaped valleys and flat floored valleys [2,19,36].

3.1.6. Mountain Front Sinuosity Index (*Smf*)

The *Smf* index is a very important indicator for evaluating the relative activity signals along the different mountain fronts. This parameter measures the tectonic/erosion balance between producing a winding line of mountain front and providing uplift signatures with relatively straight mountain fronts [21,23]. Authors in Ref. [40] define this index as:

$$Smf = \text{Lmf}/\text{Ls}$$

where Lmf measures the sinuous trace of the mountain fronts (morphological break in the slope), and Ls detects the straight-trace length of the mountain fronts [13,38] (Figure 8).

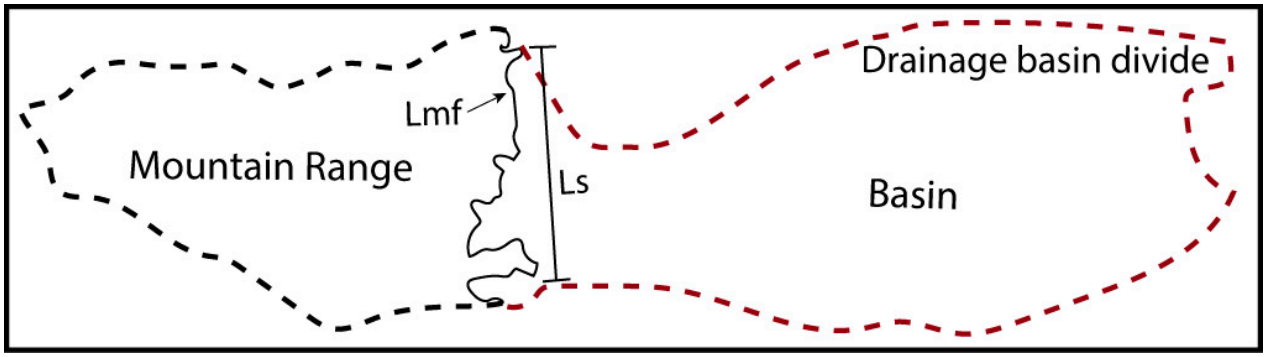

Figure 8. Figure showing the mechanism of defining mountain front sinuosity (*Smf*).

The active mountain fronts generally provide uplift signatures rather than erosional conditions.

4. Results and Discussion

4.1. Morphometric Indices

4.1.1. Stream-Length Gradient Index (*SL*)

The *SL* index values were computed over the study region using geospatial analysis from digital elevation models and are illustrated in Figure 9. In order to start analyzing the values of this index, the lithology that covers the study region was defined by different rock strength levels based on their resistance levels (Figure 9a).

The *SL* values range from less than 100 to greater than 500 along the main channels of the investigated basins. The lowest values are mostly observed over the soft rocks (Figure 9). Regarding this index, we aimed to use *SL* values to figure out the tectonic activity of basins and structural elements as well; therefore, we investigated values of the *SL* index over the different lithology, faults, and thrusting (Figure 9a,b). Quantitative values of the *SL* index linked to relative lithology resistance suggest that values provide a variable distribution over the entire study region. The analysis of the *SL* values along the SE border of the Fatima suture zone, particularly over basin 35, demonstrates the highest values of this index with moderate resistance rocks. This observation may represent the most anomalous remarks of this index. Many authors have interpreted these anomalies, where high *SL* values are not associated with hard rocks, to be tectonic activity signatures. Some locations in the study region over the northern border also present enormously high *SL* values over relatively soft rock units such as basins (40 and 41; in Figure 9a). The analysis of the *SL* index along the main Fatima suture trace reveals that low-to-medium values run parallel to the thrusting zones. At the NE border, the highest *SL* index crosses the eastern terminal of the thrusting and runs parallel to a major fault or shear zone (Figure 9b). At the SE border, moderate-to-high values were observed along a major fault or shear zone (Figure 9b). *SL* index values generally increase as streams and rivers run over active uplift spots and provide lower signals when running parallel to tectonic features such as valleys initiated by a strike-slip fault [39]. Most of the faults/shear zones carry *SL* segments with low values indicating active tectonic signals of these tectonic elements (Figure 9b).

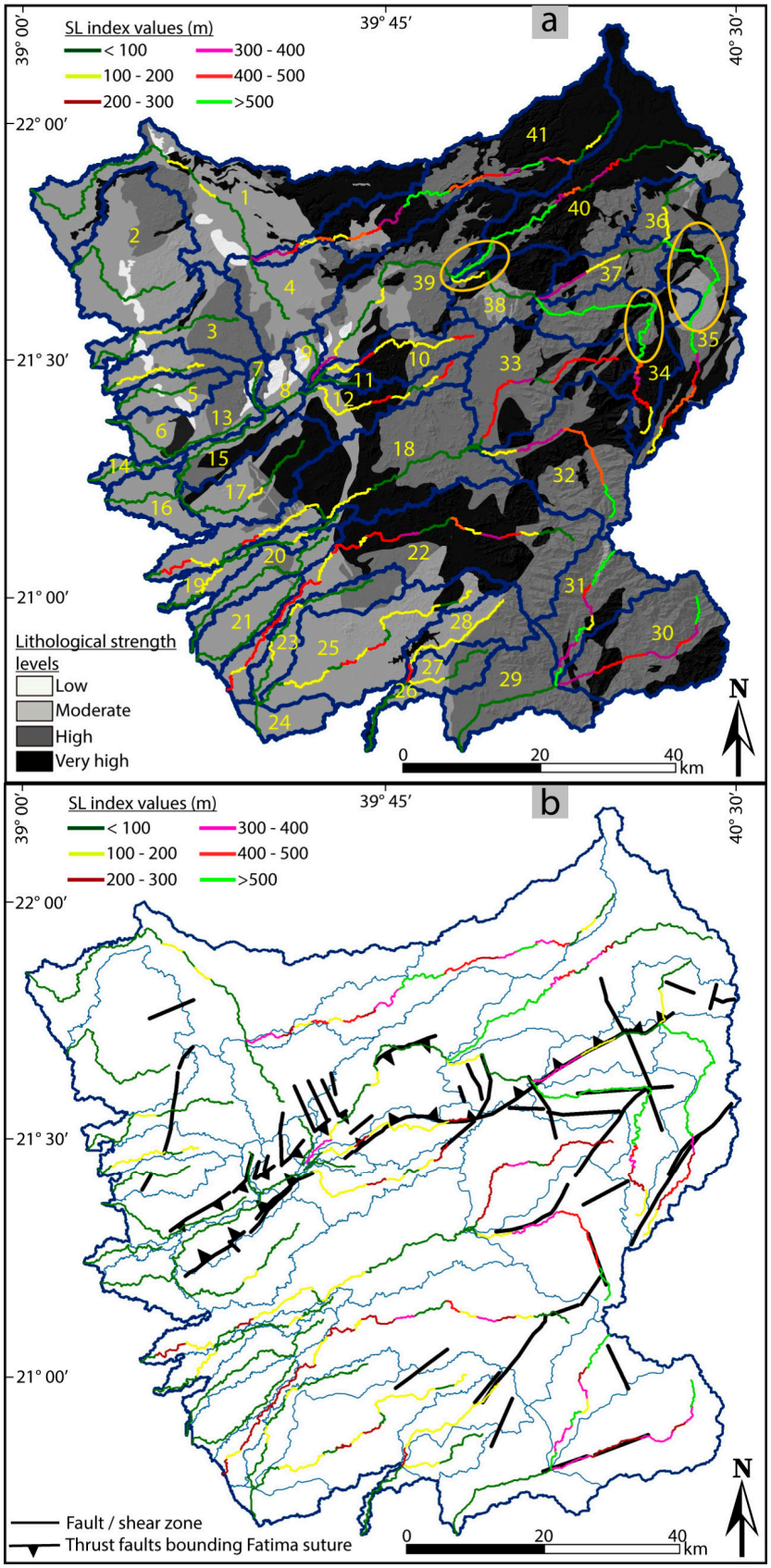

Figure 9. (**a**) SL index along the streams and geological strength levels (ellipsoidal polygons indicate the SL index anomalies), yellow numbers indicate the basin's numbers; (**b**) SL index along the tectonic elements of the study zone.

4.1.2. Asymmetry Factor Index (*Af*)

The results illustrated in Table 1 for the *Af* index include the *Af*-50 presenting the range of difference between the neutral amount of 50 and the calculated value [9,22]. Accordingly, in order to assess the relative tectonic activity, the absolute amount of difference is essentially required. The *Af*-50 values range from 0.79 to 43.37 (Table 1).

Table 1. Asymmetry factors and classes of FSZ.

Basins	*Af*	*Af*-50	Class	Basins	*Af*	*Af*-50	Class
1	72.023	22.023	1	22	47.953	−2.046	-
2	62.766	12.766	2	23	29.407	−20.952	1
3	54.703	4.703	-	24	−16.786	−33.213	1
4	57.145	7.145	3	25	62.230	12.230	2
5	84.291	34.291	1	26	44.444	−5.555	3
6	42.553	−7.446	3	27	55.977	5.977	3
7	43.710	−6.289	3	28	38.305	−11.694	2
8	77.134	27.134	1	29	55.865	5.865	3
9	56.427	15.427	1	30	58.464	8.464	3
10	39.909	−10.090	2	31	59.917	9.917	3
11	71.469	21.469	1	32	60.794	10.794	2
12	43.835	−6.164	3	33	72.083	22.083	1
13	75.270	25.270	1	34	64.013	14.013	2
14	55.501	5.501	3	35	67.248	17.248	1
15	20.477	−29.522	1	36	48.207	−1.972	-
16	50.791	0.791	-	37	40.714	−9.285	3
17	61.935	11.935	2	38	57.811	7.811	3
18	37.906	−12.093	2	39	52.899	2.899	-
19	55.054	5.054	3	40	52.964	2.964	-
20	61.198	11.198	2	41	62.363	12.363	2
21	93.379	43.379	1				

The lowest values of the *Af* index were observed for basins 16, 36, 22, 40, and 39 as 0.79, −1.97, −2.04, 2.89, and 2.96, respectively (basins do not show any tilting amount). In contrast, basin 21 located in the SW part of the study area, provides the highest value of the *Af* index (highly asymmetric basin) (Table 1 and Figure 10). The rest of the basins record values in between these two divisions (Table 1).

In order to explain the significance of the tilting amounts of the basins along the Fatima suture zone and neighboring ranges, we used the tilting amounts of the basins to arbitrarily categorize the FSZ basins into four levels indicating specific levels of relative tectonic activity: symmetrical class 0 ($Af < 5$); asymmetrical class 3 ($5 < Af < 10$); asymmetrical class 2 ($10 < Af < 15$); and asymmetrical class 1 ($15 < Af$) [8,19,20,55]. How bedding orientation is structurally governed could act an important factor in the basins' asymmetric development. Inclined amounts of bedding provide suitable conditions for valley migration in the down-dip direction providing symmetrical basins. In this study, several basins were detected to have an asymmetric index related to structural rule, and those were not considered in the index development of the relative tectonic activity. Significantly, the most asymmetric characteristics were observed along the main trace of the FSZ in the western part (basins 5, 13, and 15) and in the eastern part in basins 33 and 35 (Figure 11).

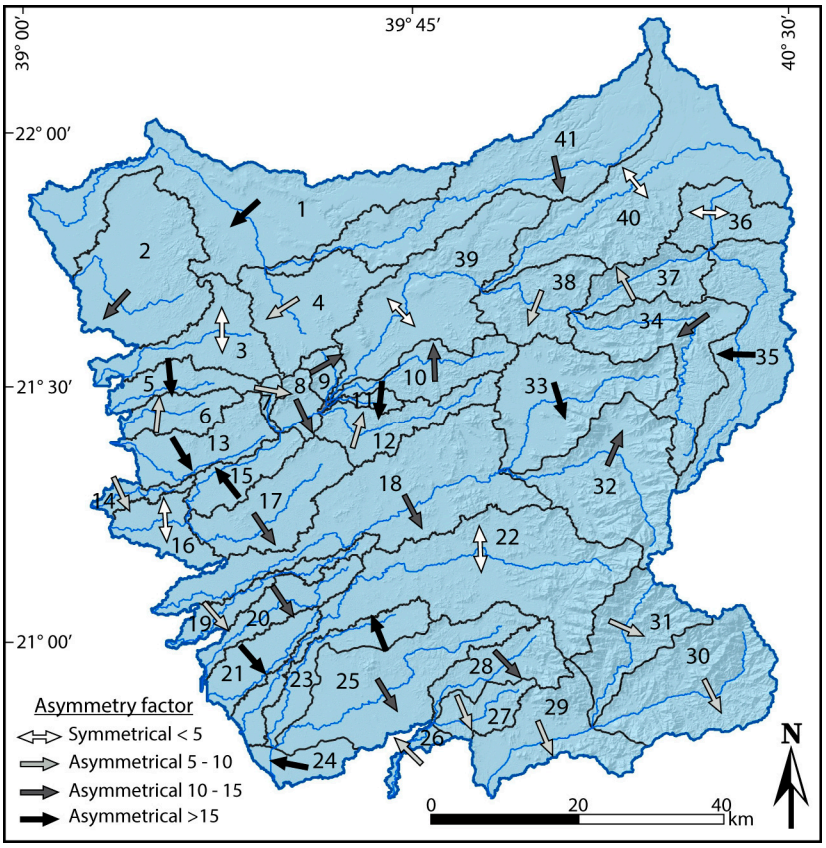

Figure 10. Figure providing the tilting amount related to tectonic activity extracted from the *Af* index.

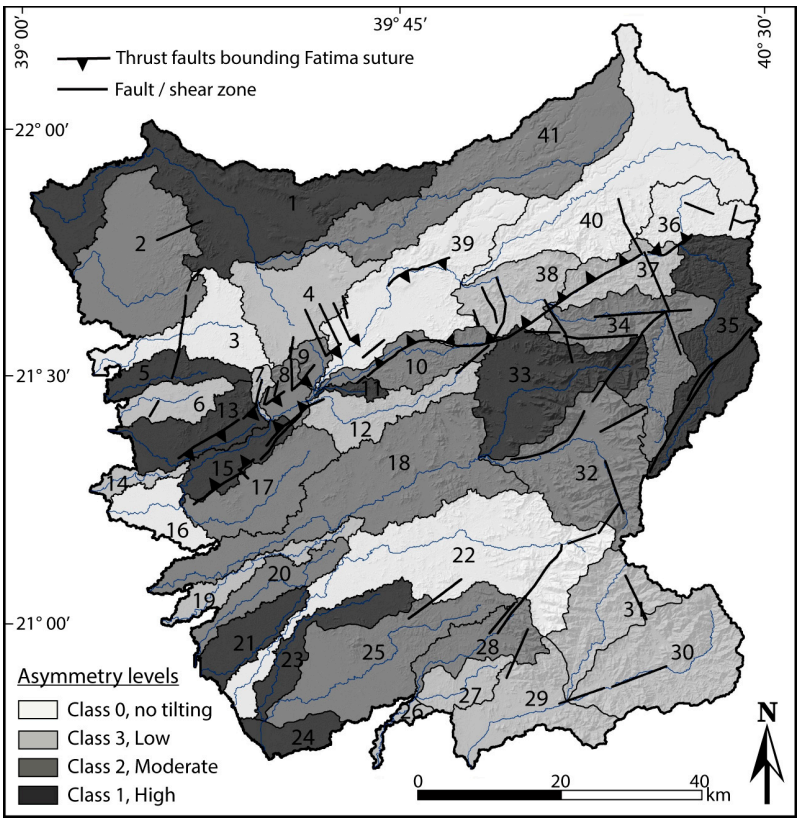

Figure 11. Relative asymmetry tectonic map produced by asymmetry classes.

4.1.3. Hypsometric Integral Index (*Hi*)

The results of the *Hi* index provide values between 0.25 and 0.64. The lowest value was observed for basin 3 in the NW part of the study region, whereas the highest result was recorded in the southern border of the study zone for basin number 23 (Figures 12 and 13). In this study, the hypsometric integral index presented an analysis of the hypsometric integral and curves. High values of the Hi index suggest prevailing conditions of younger landscapes and basins and fewer conditions of erosion processes resulting mostly from active tectonic signals [2,20,22]. In contrast, lower values of the Hi index suggest older landscapes, more signals for erosion conditions, and fewer signatures of relative tectonic uplift [9,56]. In this paper, we consider analysis of the hypsometric curves and investigate whether the curves are convex in the lower portions, convex to concave in the middle regions, or convex in the upper regions, as well as the Hi index values themselves. Many papers assume that convex curves are usually associated with high Hi values indicating uplift associated with active folds or along faults [1,2,9,19]. Generally, high Hi values are related to relatively young tectonic activity while low values of this index are extracted from landscapes that have been subjected to erosion and few impacts of recent tectonics. The Hi index was calculated for each basin, and values were defined into three groups of activity with respect to the concavity or convexity of the hypsometric curves: convex curves (class 1; Hi $\geq$ 0.5); convex–concave curves (class 2; 0.4 $\leq$ Hi < 0.49); and concave curves (class 3; Hi < 0.4). Hi index analysis of the study zone was completed based on the DEMs and utilization of all investigated basin bodies of greater than the fourth order. The analysis and results are illustrated in Figures 12 and 13. Half of the studied basins were assigned to class 2 (twenty-one basins), while classes 1 and 2 were recorded for nine and twelve basins, respectively.

4.1.4. Drainage Basin Shape Index (*Bs*)

The analysis of the drainage basin shape index (*Bs*) provides values between 0.32 and 6.22. The lowest value was calculated in basin 24, which is located in the most southern tip of the study zone. In contrast, the highest value is assigned for basin 19, which covers an area in the SE part of the study zone (Table 2; Figure 14). The analysis of this index depends mainly on a basin geometry; therefore, relatively recent basins along active zones tend to provide elongation shapes parallel to the topography of the slope of a given mountain. The scale of this index is the circularity of the basins. As tectonic activity decreases with time, the elongated basins turn into circular basins. Many papers have suggested that the reason for this transformation is because the widths of the basins are narrow close the mountain fronts over the regions characterized by tectonic activity where the stream energy has been directed mainly to down cutting; vice versa, a slow uplift allows basins to widen upstream from the given mountain fronts [2,9,23,57]. In this paper, the *Bs* index was computed for each basin, and values were categorized into three activity groups with respect to the circularity or elongation of the basins: class 1 = *Bs* $\geq$ 3 (high tectonic activity); semi-circular/semi-elongation basins class 2 = 1 $\leq$ *Bs* < 3 (moderate tectonic activity); and elongated basins class 3 = *Bs* < 1 (low tectonic activity). The analysis of this index reveals that the most elongated basins (basins 18, 19, and 20) are concentrated in the middle region parallel to the main trace of the FSZ. They are also observed in the northern (basin 41), eastern (basins 5 and 14), southern (basins 23 and 26), and western (basins 5 and 14) parts of the study region, respectively (Figure 14). Additionally, the most circular basins (low relative tectonic activity) are recorded in the NW corner of the study region, namely basins 1, 2, and 4 (Figure 13). More than half of the basins are assigned as moderate tectonic activity basins (22 basins) and nine basins have high tectonic activity, while the lowest tectonic activity basins are accounted for the remaining ten basins (Table 2; Figure 14).

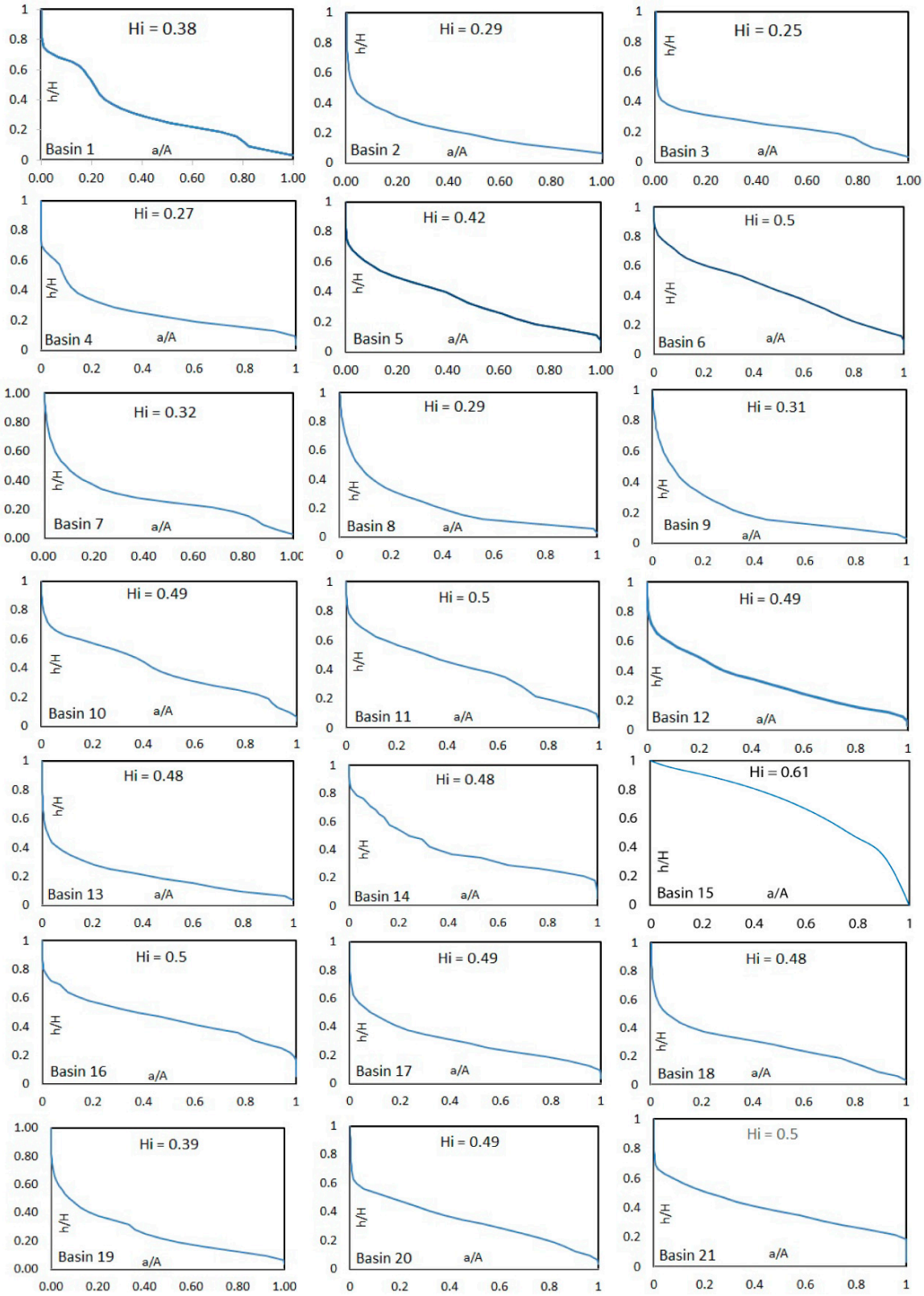

Figure 12. *Cont.*

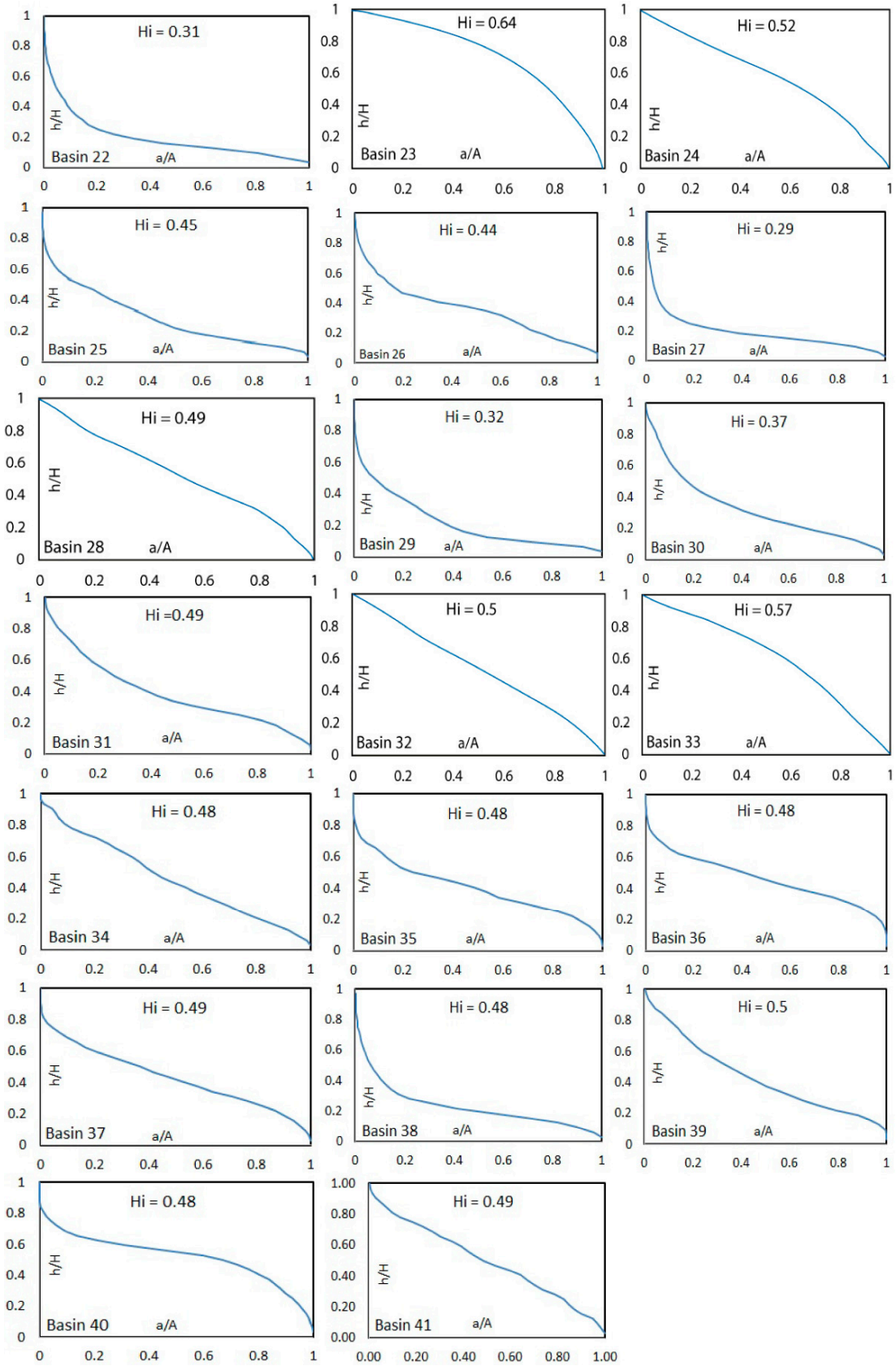

Figure 12. Hypsometric curves of basins. "A" symbol is the total area of the basin. The "a" symbol is the surface part of the basin above a given line of elevation (h). "H" symbol is the highest elevation of a given basin.

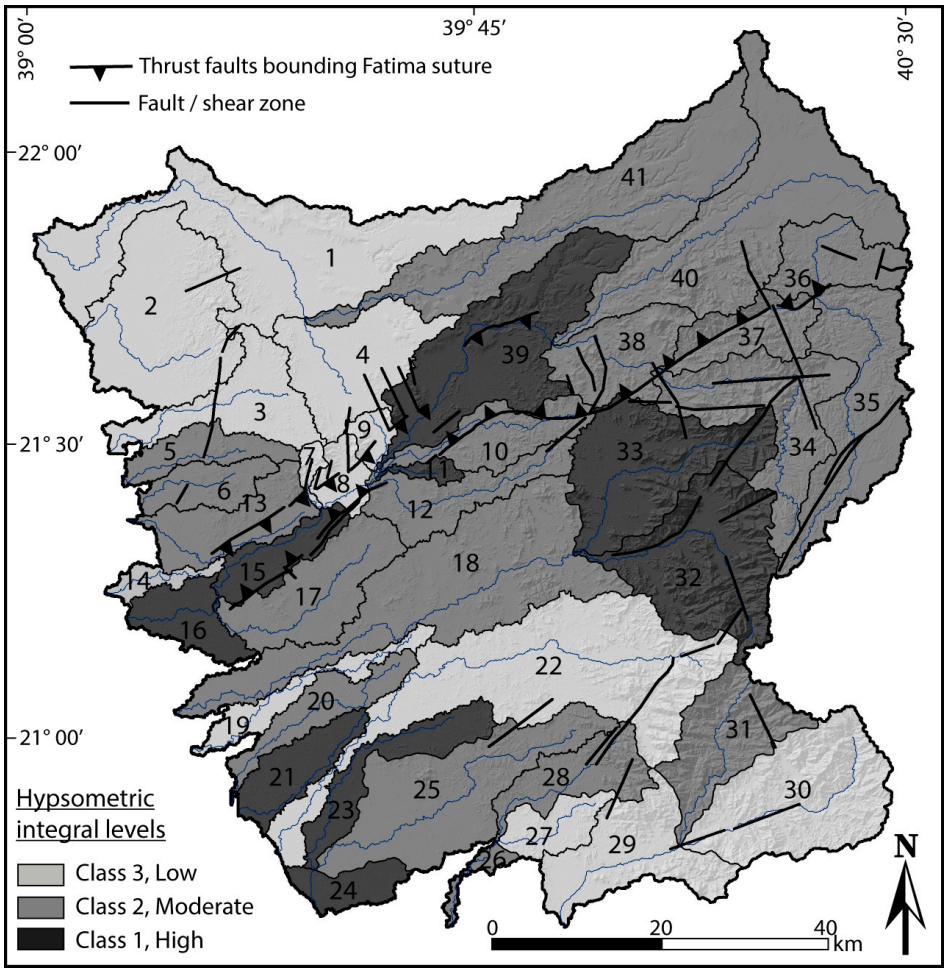

Figure 13. *Hi* tectonic activity classes of the analyzed basins.

Table 2. Values of *Bs* index in the investigated basins (Bl: basin length assigned from the headwaters to the mouth; Bw: basin width measured along its widest zone).

Basins	Bl (m)	Bw (m)	Bs	Class	Basins	Bl (m)	Bw (m)	Bs	Class
1	50,700	57,200	0.88	3	22	81,010	23,340	2.50	2
2	23,300	39,000	0.59	3	23	44,230	78,600	5.62	1
3	33,800	26,100	1.29	2	24	66,700	20,550	0.32	3
4	20,700	33,000	0.61	3	25	58,080	24,580	2.36	2
5	31,600	8890	3.55	1	26	18,000	51,600	3.48	1
6	25,600	10,200	2.5	2	27	23,020	11,000	2.09	2
7	12,400	48,600	2.55	2	28	31,880	14,900	2.13	2
8	11,000	14,700	0.74	3	29	25,610	26,250	0.97	3
9	11,300	86,500	1.30	2	30	38,990	24,490	1.59	2
10	39,700	14,300	2.77	2	31	34,030	17,720	1.92	2
11	15,510	58,400	2.65	2	32	35,500	38,450	0.92	3
12	38,660	14,080	2.74	2	33	43,070	23,380	1.84	2
13	34,000	12,530	2.71	2	34	41,590	16,670	2.49	2
14	22,050	55,700	3.95	1	35	53,710	17,500	3.06	1
15	27,500	10,660	2.57	2	36	16,460	22,980	0.71	3
16	16,060	17,930	0.89	3	37	30,610	14,860	2.05	2
17	36,100	16,220	2.22	2	38	19,220	26,240	0.73	3
18	76,990	23,630	3.25	1	39	38,930	25,020	1.55	2
19	49,060	78,800	6.22	1	40	63,310	48,320	1.31	2
20	43,200	86,800	4.97	1	41	86,740	18,520	4.61	1
21	29,920	11,700	2.55	2					

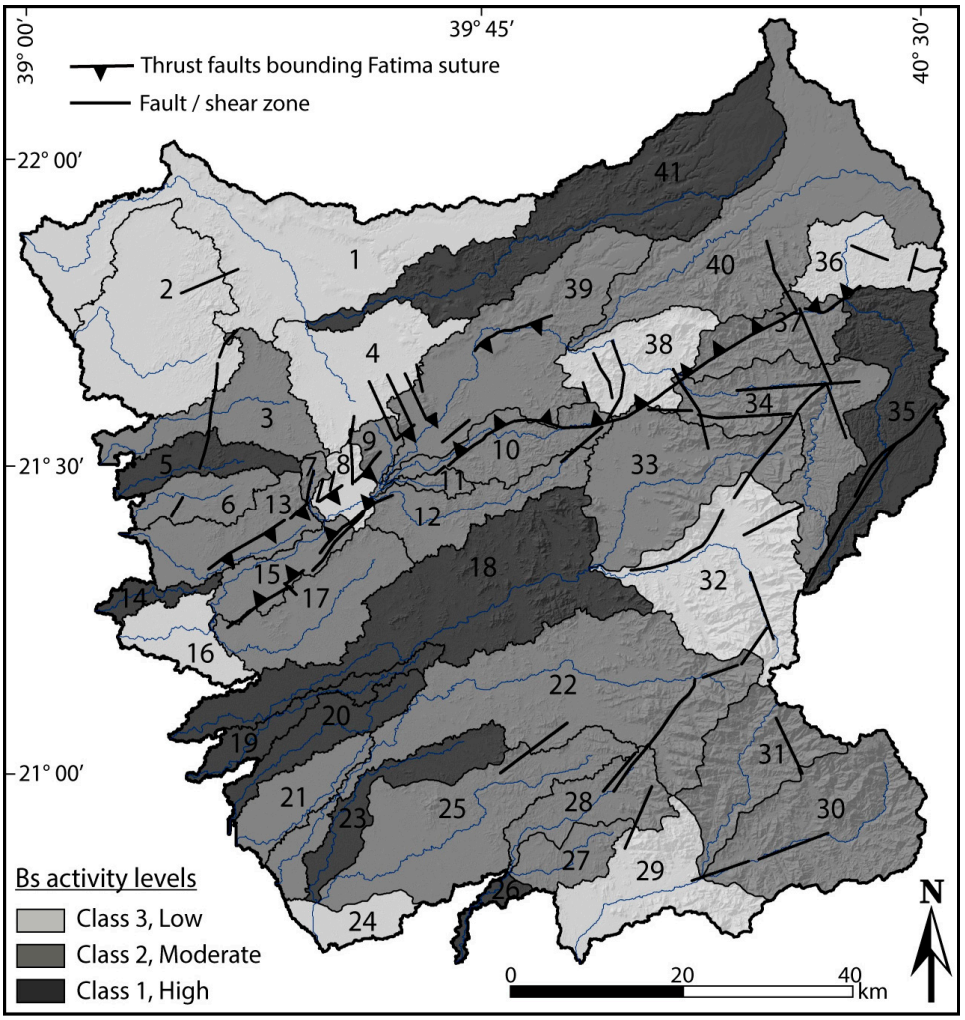

Figure 14. *Bs* tectonic activity classes of the analyzed basins.

4.1.5. Valley Floor Width-to-Height Index (*Vf*)

The results of the mean *Vf* values range from 0.3 to 3.50 all over the studied region (Table 3; Figure 15). The lower value of this index was calculated for basin 8 at the middle part of the study region along the main FSZ trace, whereas the highest was extracted from streams of basin 27 in the southern tip of the study region (Table 3; Figure 15). This particular index recognizes valleys with open floors relative to the height of their walls, providing a "U" shape and a "V" shape that defines the narrow, steep valleys [9,39]. Therefore, U-shaped valleys generally give high values of the *Vf* index, whereas valleys with a V shape have low *Vf* values. In order to discuss this index effectively, the relationship between uplift and incision is important to mention. Streams with low *Vf* values indicate active tectonic signals with high rates of incision and uplift. Accordingly, high values of this index usually provide signals of low active tectonics and no rate of incision. The values of *Vf* are calculated for the main valleys of the study region. In the general results, the *Vf* values were observed to be relatively low for most of the basins of the study region, with a small exception of the more stable areas in the southern part of the study region (Table 3; Figure 15). Values of the *Vf* index are shown in Table 3, and locations where processing of the *Vf* index were run are illustrated in Figure 15.

Table 3. Values and relative tectonic classes of *Vf* calculated in the FSZ.

Basins	*Vf*	Class	Basins	*Vf*	Class	Basins	*Vf*	Class
1	2.69	3	15	0.86	1	29	1.93	2
2	2.43	2	16	1.95	2	30	0.99	1
3	2.15	2	17	1.90	2	31	1.23	2
4	2.10	2	18	0.55	1	32	1.65	2
5	0.61	1	19	0.57	1	33	0.95	1
6	2.18	2	20	0.66	1	34	1.88	1
7	0.32	1	21	0.66	1	35	0.95	1
8	0.30	1	22	0.93	1	36	2.45	2
9	0.49	1	23	0.68	1	37	3.00	2
10	2.50	2	24	0.63	1	38	2.20	2
11	0.89	1	25	0.68	1	39	1.00	1
12	1.75	2	26	3.15	3	40	1.60	2
13	0.85	1	27	3.50	3	41	2.50	2
14	2.82	3	28	2.19	2			

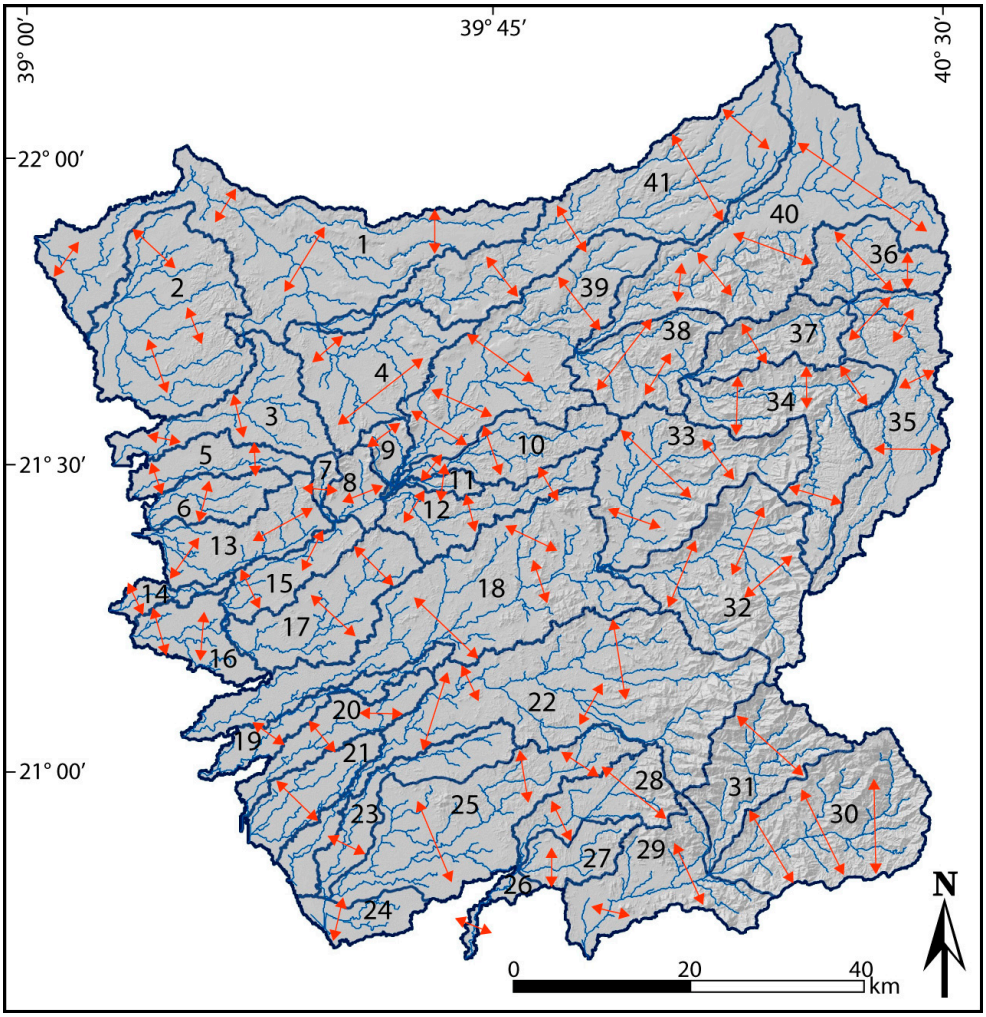

Figure 15. Location of sections for the *Vf* index calculation in the FSZ, red arrows indicate the calculated sections.

Vf values vary based on river discharge, basin size, and lithology encountered [9]. For this reason, *Vf* values should be compared for the same geological conditions [2,3]. In order to follow the general structure of this paper, *Vf* values were classified into three

levels in respect to relative tectonic activity: class 1 ($Vf \leq 1$); class 2 ($1 < Vf \leq 2.5$); and class 3 ($Vf > 2.5$), as high, moderate, and low tectonic activity, respectively (Figure 16).

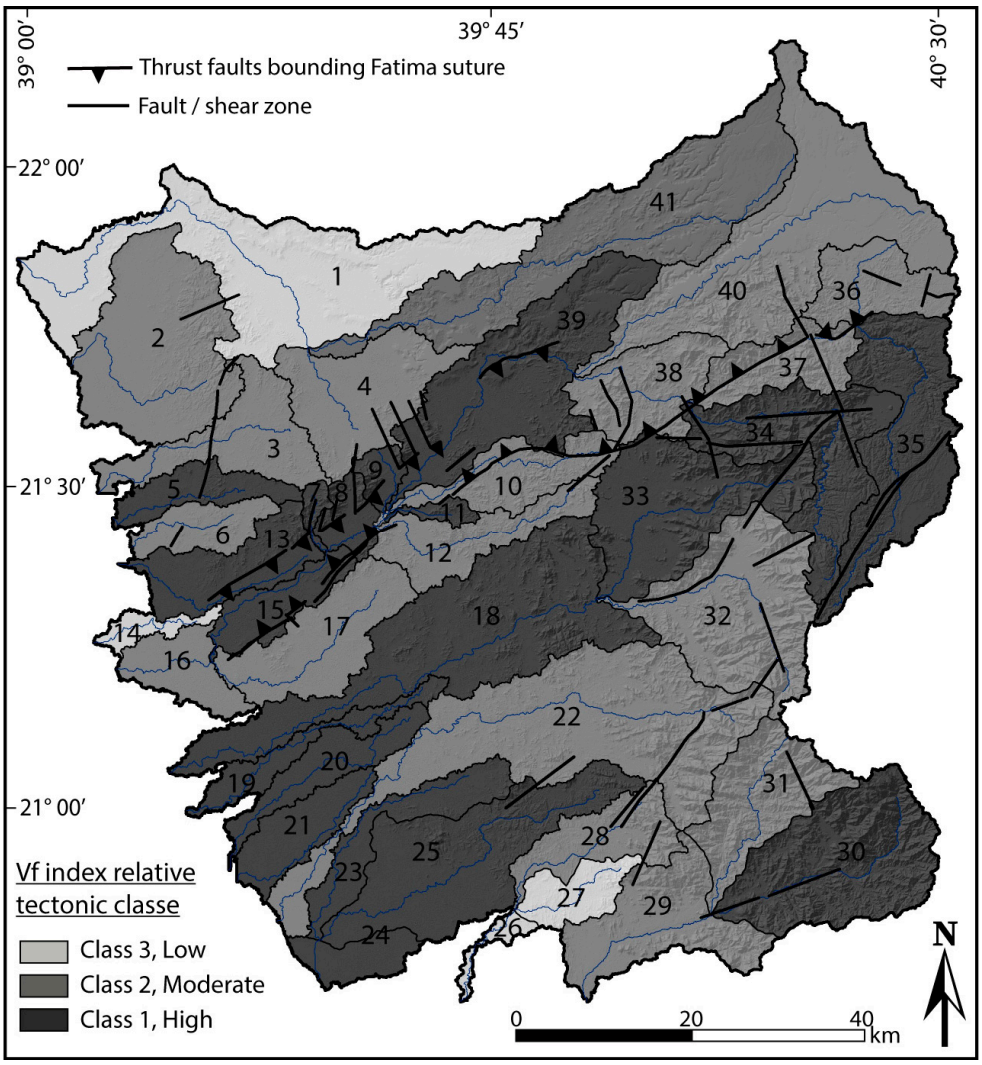

Figure 16. Relative tectonic classes map of the *Vf* index in the FSZ.

4.1.6. Mountain Front Sinuosity Index (*Smf*)

In this work, the results of the mountain front sinuosity index range from 1.0 to 2.4 along the 65 segments of mountain fronts (Table 4). The lowest value, highest value, and values between them reveal that all segments provide signatures of tectonic activity, and no inactive faults were recorded in the study region. The lowest values were recorded for segment 8 in the middle part and 41 and 50 in the eastern part of the study region, whereas the highest value was observed for segment 26 in the middle part of the study region (Figure 17). Active uplift producing straight mountain fronts generally has low values of *Smf*; when the uplift rate ceases, as long as erosional actions produce more sinuous signatures along the mountain fronts, it provides lower values of *Smf* [1,36,38]. Results of *Smf* are calculated using topographic maps, digital elevation models, or aerial photography. High resolution data with a large scale such as topographic maps are more appropriate for *Smf* assessment than other small-scale data [9,40]. Results from the *Smf* index reach 1.0 along the active fronts, whereas its values increase if the process of erosion starts to control the conditions producing irregular traces over time. In this study, *Smf* values less than 1.5 indicate active tectonic fronts, while fronts providing values greater than 2.5 belong to inactive fronts [3,38,39]. This effective index has also been applied in many regions, such as in southern Spain by authors in Ref. [9], using topographic maps, from which they

extracted values between 1.04 to 1.61. Another study was in central Anatolia, in which the author in Ref. [39], using a digital elevation model, presented values between 1.5 and 2.3. He considered values greater than 2.5 as a scale of inactive tectonic fronts and values less than 1.5 as indicative of active fronts.

Table 4. Morphometric indices of the investigated segments.

Segments	*Smf*	*Vf*	Segments	*Smf*	*Vf*	Segments	*Smf*	*Vf*
1	2.3	2.49	23	2.3	1.25	45	2.0	2.10
2	2.1	2.40	24	1.85	1.05	46	2.1	2.33
3	2.0	2.10	25	2.1	1.25	47	1.75	1.95
4	1.4	0.70	26	2.4	2.45	48	2.35	1.45
5	1.25	0.95	27	1.7	1.20	49	1.45	0.90
6	1.35	1.00	28	1.65	2.48	50	1.1	0.90
7	1.2	0.72	29	2.0	2.35	51	1.6	1.12
8	1.1	0.75	30	2.0	2.23	52	1.64	1.40
9	1.55	1.0	31	1.7	2.40	53	1.8	1.70
10	1.25	0.90	32	1.68	2.41	54	1.88	2.10
11	1.8	2.00	33	1.5	2.10	55	2.10	1.84
12	1.6	1.75	34	1.55	2.45	56	1.8	1.50
13	2.1	1.80	35	2.1	2.30	57	2.1	2.15
14	1.9	1.65	36	1.95	1.25	58	1.98	2.35
15	2.22	1.90	37	2.15	2.45	59	1.95	1.85
16	2.1	1.20	38	1.7	1.10	60	1.48	0.98
17	1.3	0.95	39	1.48	0.80	61	1.35	0.95
18	1.38	0.90	40	1.3	0.70	62	1.70	1.40
19	2.2	1.25	41	1.2	0.83	63	2.0	1.45
20	2.0	1.45	42	1.1	0.95	64	2.3	1.95
21	1.95	2.00	43	1.83	1.50	65	1.62	1.30
22	1.75	2.40	44	1.60	1.75			

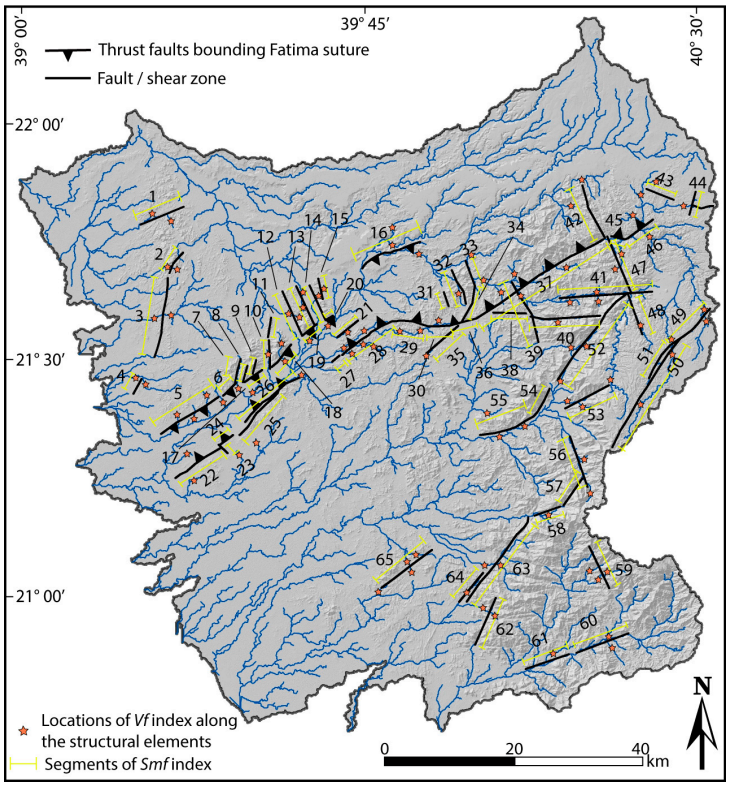

Figure 17. Figure shows the investigated 65 segments and related calculated *Vf* index.

In this study, almost all the mountain segments had relatively low *Smf* values (Table 4). The considered segments are illustrated in Figure 17 and could be sorted into two main trends of front segments: the segments along the middle zone of the study region paralleling the main trace of the FSZ (fronts such as 5, 6, 7, 8, 9, etc.) illustrate straight lines and bound the FZS, and the segments of NW–SE trend are represented by fronts (45, 47, 48, 56, and 59) giving relatively high *Smf* index values.

4.2. Relative Seismic Activity Assessment

In this study, we processed and analyzed the most effective morphotectonic indices and checked their validity in examining the relative seismic signals in regions affected by active tectonic elements previously discussed. In order to complete the tectonic assessment of the studied region, the mechanism of the morphometric indices will be discussed in this section. Several papers have applied a combination of two indices (*Smf* and *Vf*) to present such a preliminary quantitative model of relative levels of seismic activity of the examined mountain fronts. Many studies applied these two particular indices to present a chart to assign seismic activity classes [40,58]. In some recent papers, the morphometric analysis provided the designation of a chart of the *Smf* and *Vf* values, like a frequency distribution chart that illustrates the distribution of these two values along mountain fronts and major rivers crossing them [19,25,39,56]. The *Smf* values are plotted against the *Vf* values on a same chart providing three classes of relative tectonic activity. These previous papers recognize "relatively high active fronts" as those giving values of *Smf* less than 1.6 and *Vf* less than 0.5, triggered by rates of uplift ranging from 1 to 5 m/Ka. Authors in these papers also define "moderate active fronts" as values of *Smf* between 1.6 and 2.5. Authors in Ref. [38] discuss that lower rates of uplift of 0.4:0.5 m/ka were sufficient enough to keep values of the *Smf* index down to 1.4 and values of the *Vf* down to 1, and authors stated that was necessary to produce active fronts. Obviously, from the previous discussion, these researchers tried to focus on the relative seismic activity assessment along different mountain fronts, and they did not give attention to assessing areal regions with respect to the regional seismic activity.

In this paper, we dealt with the data on morphometric indices that have been analyzed in several other papers to assess the studied landscape with respect to relative seismic activity. In general, the particular indices along the mountain fronts were applied only to studies of faults, not an area [19,39]. We present here the combination diagram of *Smf* and *Vf* to provide a model of relative activity class along all faults, shears, or thrusts in the studied regions. The mountain fronts of the study zone were defined into 65 front segments (Figure 17). According to the *Smf* and *Vf* chart, the results come from all front segments of the FSZ that fall within the zone of classes 1 and 2 (Figure 18). Based on the results of this study, only 16 segments were assigned to be plotted within the high tectonic activity class, whereas the rest of the segments belong to the moderate class of the tectonic activity class (Figure 18).

In this paper, the authors followed a technique to produce a new index in order to assess the relative seismic activity (RSA) over the entire FSZ and neighboring regions. Arbitrarily, authors classified the different indices into three distinct classes: high, moderate, and low classes (Table 5). The boundaries of the applied classes vary based on which single index is being assessed; for this paper's target, we selected the limits that normally match with variance in the range of values in the applied indices (Table 5). Therefore, in order to complete the relative seismic activity model, authors arbitrary recognize a RSA average index. RSA is extracted and obtained by the average of the classes of the morphometric indices (CA) and sorted into four distinct classes, where class 4 indicates low seismic activity with values of $CA > 2.5$; class 3 reflects moderate seismic activity ($2 < CA \leq 2.5$); class 2 is high seismic activity ($1.5 < CA \leq 2$); and class 1 indicates very high seismic activity ($CA \leq 1.5$).

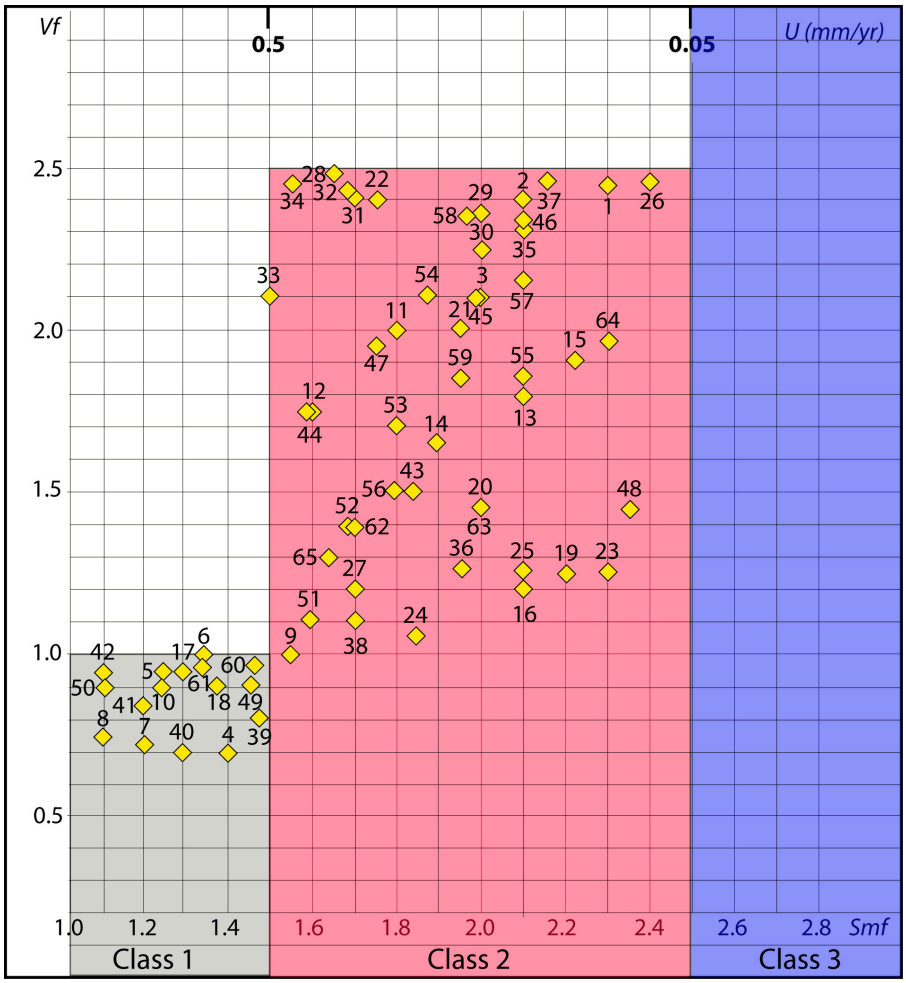

Figure 18. Figure showing plot of *Smf* and *Vf* for the mountain fronts of each single segment and activity class. Inferred rates of uplift *U* (*mm/yr*) from author in Ref. [38].

The averages of the applied indices of the seismic activity CA and RST values are presented in Table 5 for 41 basins in the study region. For the applied morphometric indices, authors have assigned three classes or levels of seismic activity, but we modified this scale by adding one more class for RTA. We added this extra class because we recognized a few tectonic geomorphology indices with unusually low values indicating greater seismic activity.

Analysis of the RSA index reveals that the low seismic activity level (high RSA class) was observed in a small area in the southern part of the study region. A very high seismic activity level was recorded for 12 basins, and high seismic activity was observed for 18 basins, while moderate seismic activity was recorded for the rest of the basins (10 basins) (Table 5). Therefore, analysis of the basins' numbers implies that 29.29% is the percent of the very high seismic basins, 43.90% is the percent of the high seismic activity level, basins of moderate seismic activity were recorded at 24.39% of the total area of the studied region, and finally, the lower seismic level was covered by only 2.43% of the study region total area (Figure 19). The distribution of the applied indices recognizes different zones associated with diverse mountain fronts and different relative rates of seismic activity (Figure 19). The high seismic activity zones cover mainly the western and southern part of the study region, while the moderate seismic activity parts are plotted in the NW and SE locations of the study region. Within the entire study region, about 36.07% (5378.29 km^2) is class 1 (very high seismic activity) as estimated by RSA; 36.62% (5469.63 km^2) reflects high seismic activity based on the RSA index (class 2); 24.66% (3677.9 km^2) presents signatures of class 3 (moderate seismic activity); and just 2.56% (383.06 km^2) compose the lowest

seismic activity class (class 4) with the lowest value of the RSA index. Therefore, two thirds of the total study area is assigned into classes 1 and 2 of very high to high seismic activity with respect to the average results from the morphometric analysis. Regarding different seismic conditions with higher rates of tectonic activity, the morphometric indices' values could vary, as could their value range [2]. Accordingly, the RSA index could also provide different values, as could the boundaries between the evaluated classes of relative seismic activity [9].

Table 5. Values of *Bs* index in the investigated basins (Bl: basin length assigned from the headwaters to the mouth; Bw: basin width measured along its widest zone).

Basins	*SL* Class	*Af* Class	*Hi* Class	*Vf* Class	*Bs* Class	*Smf* Class	CA	RSA Class
1	3	1	3	3	3	2	2.5	3
2	3	2	3	2	3	2	2.5	3
3	2	-	3	2	2	2	1.8	2
4	2	3	3	2	3	1	2.3	3
5	3	1	2	1	1	2	1.6	2
6	3	3	1	2	2	3	2.3	2
7	2	3	3	1	2	2	2.1	3
8	1	1	3	1	3	1	1.6	2
9	1	1	2	1	2	1	1.3	1
10	1	2	2	2	2	1	1.6	2
11	2	1	1	1	2	1	2.1	3
12	1	3	2	2	2	3	1.5	1
13	2	1	2	1	2	1	1.6	2
14	1	3	2	3	1	-	1.3	1
15	2	1	1	1	2	1	1.5	1
16	3	-	1	2	3	-	2	2
17	2	2	2	2	2	2	2	2
18	2	2	2	1	1	-	1.3	1
19	2	3	3	1	1	-	1.6	2
20	2	2	2	1	1	-	1.3	1
21	2	1	1	1	2	-	1.6	2
22	1	-	3	1	2	2	1.5	1
23	3	1	1	1	1	-	1.6	2
24	2	1	1	1	3	-	1.3	1
25	1	2	2	1	2	3	1.8	2
26	3	3	2	3	1	-	2	2
27	3	3	3	3	2	-	2.3	3
28	2	2	2	2	2	2	2	2
29	2	3	3	2	3	3	2.6	4
30	21	3	3	1	2	3	2.3	3
31	2	3	2	2	2	3	2.3	3
32	2	2	1	2	3	2	2	2
33	1	1	1	1	2	1	1.6	2
34	1	2	2	1	2	1	1.5	1
35	1	1	2	1	1	1	1.1	1
36	1	-	2	2	3	2	1.6	2
37	2	3	2	2	2	2	2.1	3
38	1	3	2	2	3	2	2.1	3
39	1	-	1	1	2	2	1.1	1
40	1	-	2	2	2	3	1.6	2
41	2	2	2	2	1	-	1.5	1

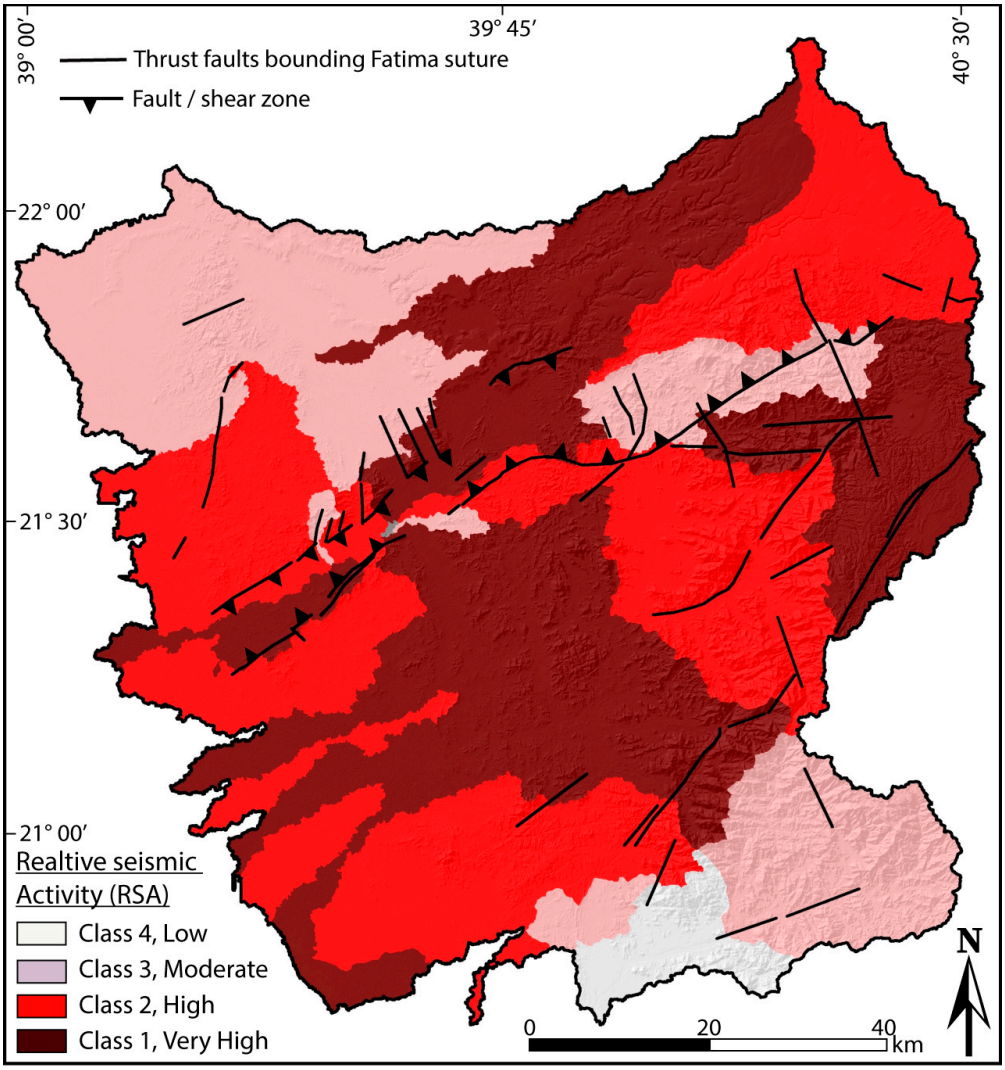

Figure 19. Figure showing the distribution of the RSA index of relative seismic activity in the FSZ and neighboring areas.

5. Conclusions

In the current paper, we present an effective method for investigating the tectonic morphology features of a highly deformed zone and its influence on the recent landscape evolution. The case study is the Fatima suture zone in western Arabia provides a very good natural laboratory for the study of the intercontinental suture zone. The conclusions of this study could be listed as:

1. Through the study of this deformed zone, the paper demonstrates the usefulness of significant geological neo-tectonic studies with morphotectonic analysis. It is also proven that the morphometric indices applied generally in vertical motion faults (*Af*, *Vf*, and *Smf*) can be successfully applied to suture structures.
2. The quantitative morphometric indices provide a very important series of geomorphic characteristics that define the study zone into different active tectonic levels that are distributed over the entire study suture zone. Additionally, these powerful indices provide the keys to processing and analyzing using remote sensing data and geospatial analysis over a vast region as an effective tool to recognize different tectonic geomorphology anomalies possible due to the behavior of seismic activity. This is particularly useful in the coastal eastern Red Sea around Mecca and Jeddah for which few studies on tectonic geomorphology based on morphometric analysis are available.

The combination of results from *Smf* and *Vf* was performed to preliminary examine the mountain fronts of the Fatima suture zone.

3. Every single morphometric index was classified arbitrarily into a number of activity classes; therefore, we applied an averaged index (RSA) that integrates all indices and classifies the studied landscape into four distinct levels of relative seismic activity. The lowest level of relative seismic activity, RSA (class 4), was observed only for one basin in the southern part of the study region, while the remaining 40 basins were distributed over the FSZ region has and have moderate, high, and very high seismic activity levels. The very high seismic activity class was recorded mainly along the thrust faults bounding the Fatima suture in the middle part of the study region. It also covers a vast area in the southern part of the study region. The high seismic activity class was observed in the eastern, western, and southern parts of the study region. The paper suggests that the southern part of the study region could provide seismic signatures rather than the northern zones. Thus, further detailed studies on quaternary chronology are required along the Fatima suture zone.
4. Finally, this paper demonstrates that morphological analysis is a very effective method for evaluating deformed structures; despite the fact that they do not produce significant topography, it provides a control on the evolution of the landscape at various scales.

Author Contributions: Conceptualization, B.B. and A.A.; methodology, B.B.; software, A.A.; validation, B.B. and A.A.; formal analysis, B.B.; investigation, A.A.; resources, B.B.; data curation, B.B.; writing—original draft preparation, B.B. and A.A.; writing—review and editing, B.B. and A.A.; visualization, B.B.; supervision, A.A.; project administration, B.B. and A.A.; funding acquisition, B.B. and A.A. All authors have read and agreed to the published version of the manuscript.

Funding: This research was supported by the Researchers Supporting Project number (RSP2023R296), King Saud University, Riyadh, Saudi Arabia.

Institutional Review Board Statement: Not applicable.

Informed Consent Statement: Not applicable.

Data Availability Statement: Not applicable.

Conflicts of Interest: The authors declare no conflict of interest.

References

1. Owen, L.A. Tectonic Geomorphology: A Perspective. In *Treatise on Geomorphology*; Elsevier: Amsterdam, The Netherlands, 2022; pp. 1–12. [CrossRef]
2. Mahmood, S.A.; Gloaguen, R. Appraisal of Active Tectonics in Hindu Kush: Insights from DEM Derived Geomorphic Indices and Drainage Analysis. *Geosci. Front.* **2012**, *3*, 407–428. [CrossRef]
3. Khalifa, A.; Çakir, Z.; Owen, L.A.; Kaya, Ş. Morphotectonic Analysis of the East Anatolian Fault, Turkey. *Turkish J. Earth Sci.* **2018**, *27*, 110–126. [CrossRef]
4. Khalifa, A.; Çakır, Z.; Kaya, Ş.; Gabr, S. ASTER Spectral Band Ratios for Lithological Mapping: A Case Study for Measuring Geological Offset along the Erkenek Segment of the East Anatolian Fault Zone, Turkey. *Arab. J. Geosci.* **2020**, *13*, 832. [CrossRef]
5. Owen, L.A. 5.2 Tectonic Geomorphology: A Perspective. In *Treatise on Geomorphology*; Elsevier: Amsterdam, The Netherlands, 2013. [CrossRef]
6. Pedrera, A.; Pérez-Peña, J.V.; Galindo-Zaldívar, J.; Azañón, J.M.; Azor, A. Testing the Sensitivity of Geomorphic Indices in Areas of Low-Rate Active Folding (Eastern Betic Cordillera, Spain). *Geomorphology* **2009**, *105*, 218–231. [CrossRef]
7. Andermann, C.; Gloaguen, R. Estimation of Erosion in Tectonically Active Orogenies. Example from the Bhotekoshi Catchment, Himalaya (Nepal). *Int. J. Remote Sens.* **2009**, *30*, 3075–3096. [CrossRef]
8. Pérez-Peña, J.V.; Azañón, J.M.; Azor, A.; Delgado, J.; González-Lodeiro, F. Spatial Analysis of Stream Power Using GIS: SLk Anomaly Maps. *Earth Surf. Process. Landf.* **2009**, *34*, 16–25. [CrossRef]
9. El Hamdouni, R.; Irigaray, C.; Fernández, T.; Chacón, J.; Keller, E.A. Assessment of Relative Active Tectonics, Southwest Border of the Sierra Nevada (Southern Spain). *Geomorphology* **2008**, *96*, 150–173. [CrossRef]
10. Cox, R.T. Analysis of Drainage-Basin Symmetry as a Rapid Technique to Identify Areas of Possible Quaternary Tilt-Block Tectonics: An Example from the Mississippi Embayment. *Geol. Soc. Am. Bull.* **1994**, *106*, 571–581. [CrossRef]

11. Cox, R.T.; Van Arsdale, R.B.; Harris, J.B. Identification of Possible Quaternary Deformation in the Northeastern Mississippi Embayment Using Quantitative Geomorphic Analysis of Drainage-Basin Asymmetry. *Bull. Geol. Soc. Am.* **2001**, *113*, 615–624. [CrossRef]
12. Keller, E.A.; Pinter, N. *Active Tectonics: Earthquakes, Uplift and Landscape*, 2nd ed.; Prentice Hall: Upper Saddle River, NJ, USA, 2002.
13. Chen, Y.C.; Sung, Q.; Cheng, K.Y. Along-Strike Variations of Morphotectonic Features in the Western Foothills of Taiwan: Tectonic Implications Based on Stream-Gradient and Hypsometric Analysis. *Geomorphology* **2003**, *56*, 109–137. [CrossRef]
14. Wells, S.G.; Bullard, T.F.; Menges, C.M.; Drake, P.G.; Karas, P.A.; Kelson, K.I.; Ritter, J.B.; Wesling, J.R. Regional Variations in Tectonic Geomorphology along a Segmented Convergent Plate Boundary, Pacific Coast of Costa Rica. *Geomorphology* **1988**, *1*, 239–265. [CrossRef]
15. Cox, R.; Garrote, J.; Swann, C.T.; Ellis, M. Tectonic Geomorphology of the Southeastern Mississippi Embayment in Northern Mississippi, USA. *Geol. Soc. Am. Bull.* **2006**, *2006*, b25721. [CrossRef]
16. Lifton, N.A.; Chase, C.; Tectonic, G. Climatic and Lithologic Influences on Landscape Fractal Dimension and Hypsometry: Implications for Landscape Evolution in the San Gabriel Mountains, California. *Geomorphology* **1992**, *5*, 77–114. [CrossRef]
17. Cyr, A.J.; Granger, D.E.; Olivetti, V.; Molin, P. Quantifying Rock Uplift Rates Using Channel Steepness and Cosmogenic Nuclide-Determined Erosion Rates: Examples from Northern and Southern Italy. *Lithosphere* **2010**, *2*, 188–198. [CrossRef]
18. Peters, G.; van Balen, R.T. Tectonic Geomorphology of the Northern Upper Rhine Graben, Germany. *Glob. Planet. Chang.* **2007**, *58*, 301–334. [CrossRef]
19. Khalifa, A.; Çakir, Z.; Owen, L.; Kaya, A. Evaluation of the Relative Tectonic Activity of the Adıyaman Fault within the Arabian-Anatolian Plate Boundary (Eastern Turkey). *Geol. Acta* **2019**, *17*, 1–17. [CrossRef]
20. Sağlam Selçuk, A. Evaluation of the Relative Tectonic Activity in the Eastern Lake Van Basin, East Turkey. *Geomorphology* **2016**, *270*, 9–21. [CrossRef]
21. Tsodoulos, I.M.; Koukouvelas, I.K.; Pavlides, S. Tectonic Geomorphology of the Easternmost Extension of the Gulf of Corinth (Beotia, Central Greece). *Tectonophysics* **2008**, *453*, 211–232. [CrossRef]
22. Khalifa, A.; Bashir, B.; Alsalman, A.; Öğretmen, N. Morpho-Tectonic Assessment of the Abu-Dabbab Area, Eastern Desert, Egypt: Insights from Remote Sensing and Geospatial Analysis. *ISPRS Int. J. Geo-Inf.* **2021**, *11*, 784. [CrossRef]
23. Partabian, A.; Nourbakhsh, A.; Ameri, S. GIS-Based Evaluation of Geomorphic Response to Tectonic Activity in Makran Mountain Range, SE of Iran. *Geosci. J.* **2016**, *20*, 921–934. [CrossRef]
24. Alipoor, R.; Poorkermani, M.; Zare, M. Geomorphology Active Tectonic Assessment around Rudbar Lorestan Dam Site, High Zagros Belt (SW of Iran). *Geomorphology* **2011**, *128*, 1–14. [CrossRef]
25. Elnobi, M.; Bashir, B.; Alsalman, A.; Bachir, H. Geospatial Analytics for Preliminarily Landscape Active Tectonic Assessment of the Wadi Araba Basin, Western Gulf of Suez, Egypt. *Appl. Sci.* **2022**, *12*, 12152. [CrossRef]
26. Bashir, B.; Alsalman, A.; Bachir, H.; Elnobi, M. GIS-Analysis for Active Tectonics Assessment of Wadi Al-Arish, Egypt. *Appl. Sci.* **2023**, *13*, 2659. [CrossRef]
27. Le Béon, M.; Klinger, Y.; Mériaux, A.S.; Al-Qaryouti, M.; Finkel, R.C.; Mayyas, O.; Tapponnier, P. Quaternary Morphotectonic Mapping of the Wadi Araba and Implications for the Tectonic Activity of the Southern Dead Sea Fault. *Tectonics* **2012**, *31*, 12. [CrossRef]
28. Bamousa, A.O.; Memesh, A.M.; Dini, S.M. Morphotectonic Development of Mesozoic Carbonates and Evaporites of Ath-Thumamah Depression in Central Arabia. *Carbonates Evaporites* **2014**, *29*, 65–72. [CrossRef]
29. Stern, R.J. Arc Assembly and Continental Collision in the Neoproterozoic East African Orogen: Implications for the Consolidation of Gondwanaland. *Annu. Rev. Earth Planet. Sci.* **1994**, *22*, 319–351. [CrossRef]
30. Harcourt-Bath, W. *The Red Sea*; Springer: Berlin/Heidelberg, Germany, 1939; Volume 177. [CrossRef]
31. Bosworth, W. Geological Evolution of the Red Sea: Historical Background, Review, and Synthesis. *Red Sea* **2015**, *3*, 45–78. [CrossRef]
32. Nofal, R.; Abboud, I.A. Geomorphological Evolution of Marine Heads on the Eastern Coast of Red Sea at Saudi Arabian Region, Using Remote Sensing Techniques. *Arab. J. Geosci.* **2016**, *9*, 163. [CrossRef]
33. Willemann, R.J.; Storchak, D.A. Data Collection at the International Seismological Centre. *Seismol. Res. Lett.* **2001**, *72*, 440–453. [CrossRef]
34. Mitchell, N.C.; Stewart, I.C.F. The Modest Seismicity of the Northern Red Sea Rift. *Geophys. J. Int.* **2018**, *214*, 1507–1523. [CrossRef]
35. El-Isa, Z.H.; Shanti, A.A. Seismicity and Tectonics of the Red Sea and Western Arabia. *Geophys. J. Int.* **1989**, *97*, 449–457. [CrossRef]
36. Azor, A.; Keller, E.A.; Yeats, R.S. Geomorphic Indicators of Active Fold Growth: South Mountain-Oak Ridge Anticline, Ventura Basin, Southern California. *Bull. Geol. Soc. Am.* **2002**, *114*, 745–753. [CrossRef]
37. Faghih, A.; Samani, B.; Kusky, T.; Khabazi, S.; Roshanak, R. Geomorphologic Assessment of Relative Tectonic Activity in the Maharlou Lake Basin, Zagros Mountains of Iran. *Geol. J.* **2012**, *47*, 30–40. [CrossRef]
38. Rockwell, T.K.; Keller, E.A.; Johnson, D.L. Tectonic Geomorphology of Alluvial Fans and Mountain Fronts near Ventura, California. In *Tectonic Geomorphology, Proceedings of the 15th Annual Geomorphology Symposium, Binghamton, NY, USA, 15 September 1985*; Allen & Unwin: Boston, MA, USA, 1985; pp. 183–207.
39. Yildirim, C. Relative Tectonic Activity Assessment of the Tuz Gölü Fault Zone Central Anatolia, Turkey. *Tectonophysics* **2014**, *630*, 183–192. [CrossRef]

40. Bull, W.B.; McFadden, L.D. Tectonic Geomorphology North and South of the Garlock Fault, California. In *Geomorphology in Arid Regions, Proceedings of the Eighth Annual Geomorphology Symposium, Binghamton, NY, USA, 23–24 September 1977*; Doehring, D.O., Ed.; State University of New York: New York, NY, USA, 1977.
41. Abd-Allah, A.M.A.; Ahmed, A.H.; El-Fakharani, A.; El-Sawy, E.K.; Ali, K.A. Fatima Suture: A New Amalgamation Zone in the Western Arabian Shield, Saudi Arabia. *Precambrian Res.* **2014**, *249*, 57–78. [CrossRef]
42. Baggazi, H.M.; Ali Abd-Allah, A.M.; Elfakharani, A.; Matsah, M. Stress-Strain Analysis and Its Tectonic Implications for the Fatima Suture Zone, Western Arabian Shield, Saudi Arabia. *J. Afric. Earth Sci.* **2019**, *158*, 103567. [CrossRef]
43. Brown, G.F.; Jackson, R.O.; Bogue, R.G.; Maclean, W.H. *Geologic Map of the Southern Hijaz Quadrangle, Kingdom of Saudi Arabia*; US Geological Survey: Reston, VA, USA, 1963.
44. Kassem, O.M.K.; Hamimi, Z. Finite Strain Analysis of the Wadi Fatima Shear Zone in Western Arabia, Saudi Arabia. *Geotectonics* **2018**, *52*, 251–265. [CrossRef]
45. Johnson, P.R.; Kattan, F. Oblique Sinistral Transpression in the Arabian Shield: The Timing and Kinematics of a Neoproterozoic Suture Zone. *Precambrian Res.* **2001**, *107*, 117–138. [CrossRef]
46. Baggazi, H.M. Paleostress Analysis of the Post-Amalgamation Fatima Basin, Western Arabian Shield, Saudi Arabia. *Arab. J. Geosci.* **2022**, *15*, 1165. [CrossRef]
47. Hargrove, U.S.; Stern, R.J.; Kimura, J.-I.; Manton, W.I.; Johnson, P.R. How Juvenile Is the Arabian–Nubian Shield? Evidence from Nd Isotopes and Pre-Neoproterozoic Inherited Zircon in the Bi'r Umq Suture Zone, Saudi Arabia. *Earth Planet. Sci. Lett.* **2006**, *252*, 308–326. [CrossRef]
48. Strahler, A.N. Quantitative Geomorphology of Drainage Basins and Channel Networks. In *Handbook of Applied Hydrology*; Chow, V.T., Ed.; McGraw Hill B. Company: New York, NY, USA, 1964; pp. 4–11.
49. Cardoso, M.; Da Silveira, A.S.; De Vargas, M.R.; De Oliveira, J.M.M.T.; Barbosa, D.V.E.; De Oliveira, L.F.B.; Fredere, A.C.; Lôndero, V. Geomorphic Expression of Shear Zones in Southern Brazilian and Uruguayan Shields. *Geomorphology* **2021**, *382*, 107678. [CrossRef]
50. Baruah, M.P.; Bezbaruah, D.; Goswami, T.K. Active Tectonics Deduced from Geomorphic Indices and Its Implication on Economic Development of Water Resources in South-Eastern Part of Mikir Massif, Assam, India. *Geol. Ecol. Landsc.* **2020**, *6*, 99–112. [CrossRef]
51. Selby, M.J. A Rock Mass Strength Classification for Geomorphic Purposes: With Tests from Antarctica and New Zealand. *Z. Für Geomorphol.* **1980**, *24*, 31–51. [CrossRef]
52. Hack, J.T. Stream-Profile Analysis and Stream-Gradient Index. *J. Res. U. S. Geol.* **1973**, *1*, 421–429.
53. Hare, P.W.; Gardner, T.W. Geomorphic Indicators of Vertical Neotectonism along Converging Plate Margins, Nicoya Peninsula, Costa Rica. *Tecton. Geomorphol.* **1985**, *4*, 123–134.
54. Ramírez-Herrera, M. Geomorphic Assessment of Active Tectonics in the Acambay Graben, Mexican Volcanic Belt. *Earth Surf. Process. Landforms* **1998**, *23*, 317–332. [CrossRef]
55. Azañón, J.M.; Pérez-Peña, J.V.; Giaconia, F.; Booth-Rea, G.; Martínez-Martínez, J.M.; Rodríguez-Peces, M.J. Active Tectonics in the Central and Eastern Betic Cordillera through Morphotectonic Analysis: The Case of Sierra Nevada and Sierra Alhamilla. *J. Iber. Geol.* **2012**, *38*, 225–238. [CrossRef]
56. Khalifa, A. Preliminary Active Tectonic Assessment of Wadi Ghoweiba Catchment, Gulf of Suez Rift, Egypt, Integration of Remote Sensing, Tectonic Geomorphology, and Gis Techniques. *Al-Azhar Bull. Sci.* **2020**, *31*, 35–42. [CrossRef]
57. Buczek, K.; Górnik, M. Evaluation of Tectonic Activity Using Morphometric Indices: Case Study of the Tatra Mts. (Western Carpathians, Poland). *Environ. Earth Sci.* **2020**, *79*, 176. [CrossRef]
58. Silva, P.G.; Goy, J.L.; Zazo, C.; Bardají, T. Faulth-Generated Mountain Fronts in Southeast Spain: Geomorphologic Assessment of Tectonic and Seismic Activity. *Geomorphology* **2003**, *50*, 203–225. [CrossRef]